Draft version September 3, 2012
Preprint typeset using LaTeX style emulateapj v. 11/26/04

PULSATION FREQUENCIES AND MODES OF GIANT EXOPLANETS

Bastien Le Bihan[1,2] & Adam Burrows[1]

Draft version September 3, 2012

ABSTRACT

We calculate the eigenfrequencies and eigenfunctions of the acoustic oscillations of giant exoplanets and explore the dependence of the characteristic frequency ν_0 and the eigenfrequencies on several parameters: the planet mass, the planet radius, the core mass, and the heavy element mass fraction in the envelope. We provide the eigenvalues for degree l up to 8 and radial order n up to 12. For the selected values of l and n, we find that the pulsation eigenfrequencies depend strongly on the planet mass and radius, especially at high frequency. We quantify this dependence through the calculation of the characteristic frequency ν_0 which gives us an estimate of the scale of the eigenvalue spectrum at high frequency. For the mass range $0.5 \leq M_P \leq 15\ M_J$, and fixing the planet radius to the Jovian value, we find that $\nu_0 \sim 164.0 \times (M_P/M_J)^{0.48}\ \mu Hz$, where M_P is the planet mass and M_J is Jupiter's mass. For the radius range from 0.9 to 2.0 R_J, and fixing the planet's mass to the Jovian value, we find that $\nu_0 \sim 164.0 \times (R_P/R_J)^{-2.09}\ \mu Hz$, where R_P is the planet radius and R_J is Jupiter's radius. We explore the influence of the presence of a dense core on the pulsation frequencies and on the characteristic frequency of giant exoplanets. We find that the presence of heavy elements in the envelope affects the eigenvalue distribution in ways similar to the presence of a dense core. Additionally, we apply our formalism to Jupiter and Saturn and find results consistent with both the observationnal data of Gaulme et al. (2011) and previous theoretical work.

Subject headings:

1. INTRODUCTION

Pulsation frequencies and modes are potentially useful tools with which to study the interior structure of the giant planets. Three types of modes are distinguished: g-modes are standing internal gravity waves, p-modes are standing acoustic waves, and f-modes are of intermediate frequency and can be regarded as the fundamental mode of either the p- or the g-modes. The corresponding frequencies are characterized by their radial order n and degree l. Several forcing mechanisms may excite these modes, making them, in principle, accessible to direct observation (Bercovici & Schubert 1987; Marley 1990). However, the surface movements associated with such pulsations are hard to detect and, as of July 2012, only Jupiter's global oscillations have been observed. The work of Schmider et al. (1991), Mosser et al. (1991), Mosser et al. (1993), and Mosser et al. (2000) resulted in a measurement of the mean frequency spacing of $142 \pm 3\ \mu Hz$ (Mosser et al. 2000). More recently, Gaulme et al. (2011), using the SYMPA Fourier spectro-imager, detected Jupiter's global modes with a mean noise level five times lower than previously achieved. Their observations suggest a mean spacing of $155.3 \pm 2.2\ \mu Hz$.

Given current technological limitations to the observation of giant planet's oscillations, it is reasonable to think that the global oscillations of giant exoplanets will not be detected in the foreseeable future. However, a theoretical exploration of the systematics of the pulsation frequencies for the broad spectrum of recently discovered giant exoplanets might stimulate observers to design methods to detect giant planet oscillations, since such oscillations are so diagnostic of structure.

In this spirit, we calculate the eigenfrequencies and eigenfunctions of the pulsationnal modes of giant exoplanets. We quantify the dependence of the modal eigenfrequencies on the planet mass and radius. In addition, we focus on the influence of a dense core on these quantities, since its presence has already been suggested in specific extrasolar giant planets (Burrows et al. 2007; Guillot et al. 2006). Furthermore, we calculate corresponding models for Jupiter and Saturn themselves, and compare them with previous work.

Vorontsov et al. (1976), Vorontsov & Zarkhov (1981 a,b) and Vorontsov (1981) added rotation, differential rotation, and ellipticity to their initial spherically-symmetric, nonrotating Jovian models. The influence of the troposphere on the high-frequency oscillations was first adressed by Vorontsov et al. (1989), then in detail by Mosser et al. (1994). Provost et al. (1993) developed an asymptotic method to determine the eigenfrequencies which included the discontinuity of a Jovian core. They introduced the mean spacing or characteristic frequency ν_0, defined by: $\nu_0 = \left[2 \int_{planet} \frac{dr}{c_0}\right]^{-1}$, where c_0 is the speed of sound, and emphasized the sensitivity of the Jovian oscillation spectrum to the presence of a dense core. Since then, the Jovian characteristic frequency has been estimated to be between 152 and 160 μHz (Provost et al. 1993; Gudkova et al. 1995; Gudkova & Zarkhov 1999). These estimates are consistent with the recent observations of Gaulme et al. (2011).

Saturn's oscillations have also been studied theoretically. Marley (1990) suggested that the f-modes of Saturn are the most likely to be detected through their po-

[1] Department of Astrophysical Sciences, Princeton University, Princeton, NJ 08544 USA
[2] École Polytechnique, 91128 Palaiseau, France
Electronic address: bastien.le-bihan@polytechnique.edu, burrows@astro.princeton.edu

tential influence on that planet's rings. Using the techniques applied to Jupiter, Gudkova et al. (1995) calculated the eigenfrequencies of the lowest-order p-modes of Saturn, along with their characteristic frequencies. The latter were found to be between 106 and 109 μHz.

Throughout our paper, we highlight the general systematics and do not take into account the effects of rotation or oblateness (Vorontsov & Zarkhov 1981 a,b; Lee 1993). Since the adiabatic approximation is appropriate for Jovian planets (Marley 1990), adiabaticity is here assumed for Jupiter, Saturn, and the entire set of exoplanets. Finally, since we focus on the giant exoplanet regime, we select the appropriate range of measured giant planet radii (Udry & Santos 2007): $0.8\ R_J \lesssim R_P \lesssim 2.1\ R_J$.

Gaulme et al. (2011) and Schmider et al. (1991) suggest that the lowest-degree p-modes are the most likely to be detected. Gaulme et al. (2011) and Marley (1990) take the degree $l = 8$ to be an upper limit and the Jovian observations of Gaulme et al. (2011) are within the frequency regions [0.8, 2.1] mHz and [2.4, 3.4] mHz. In the specific case of Jupiter, and for $l \in [0, 8]$, these values loosely correspond to the ranges of radial order $n \in [0, 12]$ and [15,20], respectively. Theoretically, the asymptotic trends are manifest for $n \geq 4$ or 5 (Provost et al. 1993; Marley 1990). Thus, we focus on the p-modes and f-modes of low degree ($l \leq 8$) and relatively low radial order ($n \leq 12$).

In §2, we summarize the theory of adiabatic nonradial oscillations of nonrotating spherically planetary models. We present our numerical technique, closely based on the work of Unno et al. (1989) and Christensen-Dalsgaard (1997). To test the validity and precision of our code, we calculate the eigenfrequencies of f-modes, p-modes and g-modes of well-studied polytrope models and compare our results to those of Christensen-Dalsgaard & Mullan (1994).

In §3, we describe the giant planet models used in the article. We present our results in the case of Jupiter and Saturn, and compare them to both observationnal data (Gaulme et al. 2011) and theoretical work (Provost et al. 1993; Mosser et al. 1994; Gudkova & Zarkhov 1999). We briefly focus on the dependence of the Jovian modal oscillations on the core mass of Jupiter and present the derivatives of the low-degree acoustic modes eigenfrequencies with respect to the core mass.

In §4, we focus on the giant exoplanets. We present our results in terms of the characteristic frequency ν_0, the eigenfrequencies of low-degree f-modes, and the eigenfrequencies of low-degree p-modes across the giant exoplanet continuum. In separate subsections, we investigate their dependence on the planet mass, planet radius, and core mass. We also focus on the influence of a high fraction of heavy elements in the envelope, by using a high helium mass fraction, Y, as an approximate substitute (Spiegel et al. 2011). Finally, we briefly discuss the temporal evolution of the charateristic frequency ν_0 for simple planetary models considered in isolation.

2. METHODOLOGY AND TECHNIQUES

2.1. *Nonradial Oscillation Eigenvalue Problem*

We considered non-rotating, spherically-symmetrical planetary models. For adiabatic, nonradial oscillations of such objects, it follows from Unno et al. (1989, chap. 13) that the radial part of the displacement ξ_r, the Eulerian perturbations of the pressure p', and the Eulerian perturbation of the gravitational potential Φ' take the form:

$$f(t, r, \theta, \phi) = f(r) Y_l^m(\theta, \phi) e^{i\sigma t}, \tag{1}$$

for $f = \xi_r$, p' and Φ'. A given oscillation mode is, thus, described by its azimuthal order m, degree l, radial order n.

These variables are govern by a set of differential equations and four boundary conditions, two at the surface, and two at the center (Unno et al. 1989). The corresponding set of equations is given in the first section of the Appendix. Since the azimuthal order m does not appear in the governing equations, the eigenfrequencies are $(2l+1)$-fold degenerate, and are fully described by their degree l and radial order n.

This problem has to be numerically implemented to calculate the corresponding eigenfrequency $\nu_{n,l}$ for a given mode. We detail the technique used in this paper in the Appendix, but summarize our overall methodology in the next subsections.

2.2. *Numerical Implementation*

Several numerical techniques have been previously introduced (Vorontsov et al. 1976; Unno et al. 1989; Christensen-Dalsgaard 1997). They are divided into shooting techniques and relaxation methods. In the shooting technique, solutions satisfying the boundary conditions are integrated separately from the inner and outer boundaries, and the eigenvalue is found by matching these solutions at an arbitrary interior fitting point. The second technique is to solve the equations together with the normalization condition, and all but one of the boundary conditions, using a relaxation technique; the eigenvalue is then found by requiring that the remaining boundary condition be satisfied. The shooting methods are generally considerably faster than the relaxation techniques, but their precision decreases as the degree l increases (Christensen-Dalsgaard 1997, 2003). However, since we consider only low-degree modes, a shooting method is quite suitable for our problem. Dimensionless variables are introduced (see the second section of the Appendix). In particular, the dimensionless frequency ω is defined by:

$$\omega^2 = \frac{\sigma^2 R^3}{GM} = \frac{4\pi^2 \nu^2 R^3}{GM}. \tag{2}$$

Solutions are obtained by integration using a fifth-order Runge-Kutta technique. To calculate the eigenfrequencies in a given frequency range, we use a determinant method developed in Christensen-Dalsgaard (1997) and fully described in the third section of the Appendix. Two linearly independent solutions are calculated from the center, and two from the surface. They are connected at an arbitrary inner boundary. The eigenvalues do not depend on its position.

2.3. *Mode Order*

As we calculate the eigenfrequencies and eigenfunctions of the acoustic modes for a given degree l, we determine their order n using the following equation (Christensen-Dalsgaard 1997):

$$n = \sum_{x_{z1}>0} sign\left(y_2 \frac{dy_1}{dx}\right) + n_0\ , \tag{3}$$

where y_1 and y_2 are dimensionless variables defined by:

$$y_1 = \frac{\xi_r}{r},$$
$$y_2 = \frac{1}{gr}\left(\frac{p'}{\rho} + \Phi'\right), \tag{4}$$

where ρ is the density and g is the gravitational acceleration.

In the definition of n, the sum is over the zeros x_{z1} in y_1 (excluding the center), where $x = r/R$ is the relative radius. The value of n_0 depends on the behavior of the solution close to the innermost boundary. If y_1 and y_2 have the same sign at the innermost mesh point, excluding the center, $n_0 = 0$. Otherwise $n_0 = 1$. In particular, for a complete model that includes the center, as in our case, it follows from the boundary conditions at the center that $n_0 = 1$ for radial oscillations and $n_0 = 0$ for non-radial oscillations.

2.4. *Results for a Polytrope Model*

In order to test the code, we compute the eigenfrequencies and eigenfunctions of polytropic models. To compare our results with the work of Christensen-Dalsgaard & Mullan (1994), we take the same radius and mass for our calculations: $R_P = 6.9599 \times 10^{10}\ cm$ and $M_P = 1.989 \times 10^{33}\ g$. The eigenfrequencies of f-modes, g-modes, and p-modes are given in Tables 1, 2 and 3, in μHz. Our frequencies match those of Christensen-Dalsgaard & Mullan (1994) to a precision of 10^{-5} or better, for all types of modes, for $l \in [0, 3]$ and $n \in [-20, 25]$. This gives us confidence in our calculational method as we approach more complex models.

3. JUPITER AND SATURN

3.1. *The Models*

The giant planet models we use for the calculations for Jupiter and Saturn consist of an adiabatic atmosphere, a hydrogen-helium envelope, and an olivine core. When a core is included, we explore $0 \leq M_{core} \leq 10\ M_\oplus$ for Jupiter and $9 \leq M_{core} \leq 22\ M_\oplus$ for Saturn. Both ranges are marginally consistent with the core accretion formation models for these planets, which suggest $10 - 20 M_\oplus$ (Saumon & Guillot 2004; Pollack 1996). The hydrogen/helium equation of state that we use for this study is described in Saumon, Chabrier, & Van Horn (1995). The transition between the atmosphere and the envelope has been smoothed to ensure the continuity of density, pressure, and sound speed.

We build several models for both Jupiter and Saturn, using different core masses and helium fractions in the envelope. Table 4 presents various parameters of these models: the helium mass fraction inside the envelope, Y, the mass of the core, M_{core} (in Earth units), the central pressure p_c (in Mbars), the central density ρ_c (in cgs units), and the characteristic frequency ν_0 (in μHz), defined in Provost et al. (1993) using the following equation:

$$\nu_0 = \left[2 \int_{planet} \frac{dr}{c_0}\right]^{-1}, \tag{5}$$

where $c_0 = \sqrt{(dp_0/d\rho_0)_{ad}}$ is the sound speed in hydrostatic equilibrium.

Figure 1 portrays the profiles of the density, ρ, the gravitational acceleration, g, and the sound speed, c_0, for models J4 and S2, defined in Table 4. Both density and sound speed are discontinuous at the core interface. In the case of Jupiter, for the models defined in Table 4, the calculated characteristic frequencies, ν_0, are consistent with the observational value measured by Gaulme et al. (2011): $\nu_0 = 155.3 \pm 2.2\ \mu Hz$ (see also Figure 6).

3.2. *Oscillation Modes*

Figure 2 depicts the eigenfrequencies of models S2 and J4 for $l \in [0, 3]$ and n up to 25. These results are given in the form of échelle diagrams based on the results of the asymptotic theory for low-degree oscillations developed in, for example, Provost et al. (1993). This theory predicts that, for low degree l and large radial order n, the eigenfrequencies $\nu_{n,l}$ of p-modes are, to a first approximation, proportionnal to the characteristic frequency, ν_0:

$$\nu_{n,l} \simeq \left(n + \frac{l}{2}\right)\nu_0\ . \tag{6}$$

An échelle diagram presents the ratio $\nu_{n,l}/\nu_0$ as a function of the difference $\nu_{n,l}/\nu_0 - (n + E[l/2])$, where E is the floor function. Thus, it allows us to see the deviation from the approximate value. Both panels of Figure 2 are in qualitative agreement with previous numerical results for Jupiter (Provost et al. 1993; Mosser et al. 1994, and their Fig. 3d & Fig. 5a, respectively) and for Saturn (Mosser et al. 1994, their Fig. 5b). The Jovian periods of the acoustic fundamental tone and overtones with radial order and degree up to 5 are given in Table 5 for the model J4. Though the differences between our models and those derived by Gudkova & Zarkhov (1999) prevent us from a precise comparison, it is clear that we find similar results to this previous work (see their Table 2).

Figure 3 portrays the radial component of the eigendisplacement ξ_r for low-degree, lowest-order modal oscillations of the model J4 of Jupiter, as a function of the relative radius $x = r/R$. The radial displacement is shown for $l = 0$, 1, 2, and 5. It is taken equal to 1 m at the surface, for every mode. The behavior of the modes near the center is determined by the boundary conditions of the specific numerical problem considered here (Unno et al. 1989), which lead to the following relations, for $r \sim 0$:

$$\xi_r \sim 0 \qquad \text{for } l = 0\ ,$$
$$\xi_r \propto \left(\frac{r}{R}\right)^{l-1} \quad \text{for } l \geq 1\ . \tag{7}$$

Thus, for $l = 1$, the radial displacement does not necessary vanish near the center. In Figure 3, for the lowest degrees l, the presence of the dense core is directly visible at the boundary with the envelope ($x = 0.13$, for this model). For higher degree (here, $l = 5$), the influence of the core is less obvious in the radial eigenfunctions, because the amplitude of the radial displacement vanishes near the center, for every radial order n.

The influence of the size of the core on the frequency spectrum of Jupiter has already been studied (Provost et al. 1993; Gudkova & Zarkhov 1999). However, no determination of the derivative of the eigenfrequencies with respect to the core mass has yet been provided. Focusing on the f-modes and p-modes of Jupiter, we calculate their

eigenfrequencies for various core masses, with the helium mass fraction fixed at 0.25 in the envelope. An échelle diagram of the eigenfrequencies of Jupiter for $l = 2$ and for a few core masses is given in Figure 4. The spectra are very well separated for radial order $n \geq 4$, which indicates, as mentionned by Vorontsov et al. (1989) and Gudkova & Zarkhov (1999), that the high-frequency acoustic oscillations of low degree l can be very useful in determining the structure and size of the core.

We highlight the sensitivity to the core mass of the eigenfrequencies of low-degree acoustic oscillations. Figure 5 shows the eigenfrequencies of such modes for Jupiter as a function of the mass of the core, M_c, for $n \in [0, 10]$ and for $l = 0$, 1, 2 and 3. For every radial order n, the eigenfrequencies have been normalized by their coreless value:

$$\mu_{n,l}(M_{core}) = \frac{\nu_{n,l}(M_{core})}{\nu_{n,l}(0)} \ . \tag{8}$$

This normalization allows us to compare the deviation of the frequencies from their coreless values as the core mass increases, regardless of their absolute value, which depends of the radial order n.

For $l = 0$, as n increases the frequency becomes less sensitive to the size of the core. The normalized frequency $\mu_{1,0}$ is by far the most affected by the variation of the core mass; its value decreases by more than 14% between the coreless version of Jupiter and the model with a 10- Earth mass core. For $l \geq 1$, the trend is very different; the derivative of the normalized frequency with respect to the core mass decreases from positive to negative values as n increases. As a result, this derivative approximately vanishes for specific frequencies, for example $\mu_{3,1}$ (Fig.5, top right), $\mu_{2,2}$ (Fig.5, bottom left), and $\mu_{2,3}$ (Fig.5, bottom right). All these frequencies vary by less than 0.5% over a core mass range from 0 to 10 $M_\oplus$. For higher radial order, the influence of the core mass is more important; for example, $\mu_{10,2}$ varies by more than 3.0% over the core mass range from 0 to 10 $M_\oplus$. This increased sensitivity is consistent with the previous discussion concerning the échelle diagram. The f-mode is also sensitive to the core mass, with a variation up to 3.8% with core mass from 0 to 10 $M_\oplus$, for $l = 2$ and 3. We conclude that, for nonradial oscillations ($l \geq 1$), the sensitivity of the pulsation frequencies to the core mass is important both for the f-modes and for the high-radial order p-modes. For specific intermediate values of radial order n, the sensitivity vanishes over the whole core mass range shown. If detected, these modes would provide little evidence of the presence of a core.

4. THE GIANT EXOPLANETS

4.1. *General description*

For a systematic look at the exoplanets currently known, we use the catalog developed by Schneider et al. (2011) and available at the URL *http://www.exoplanet.eu*. As of the 7^{th} of July, 2012, 777 confirmed planets are listed in this catalog. We limit our study to the planets whose radius and mass have both been estimated. Furthermore, we focus on the giant exoplanet regime and, therefore, we select the planets whose radii are within the range $0.8\ R_J \lesssim R_P \lesssim 2.1\ R_J$. In terms of mass, most of the detected giant exoplanets have masses less than 5 M_J, but the distribution has a long tail towards masses larger than 10 M_J (Udry & Santos 2007). Numerically, 88% of the selected exoplanets have masses less than or equal to 5 M_J, and 94% have masses less than or equal to 10 M_J. In the 10 to 20 M_J interval, it is difficult to fix a clear upper limit for giant exoplanets masses, because the planet population and the brown dwarf population overlap (Udry & Santos 2007; Leconte et al. 2009). Therefore, though we restrict the mass range studied, we are aware of the ambiguous status of the heaviest objects. This final set is composed of 174 exoplanets.

We calculate the characteristic frequency ν_0 for each object of this group, using the techniques and models developed and described in sections 2 and 3. The helium mass fraction is fixed at 0.25 in the entire envelope and no core is added. The results are shown in Table 6, with the planets sorted from low to high mass. For the selected objects, the characteristic frequency range is $33\ \mu Hz \leq \nu_0 \leq 815\ \mu Hz$. Around 1 M_J, ν_0 is smaller than Jupiter's value for almost every object, since their radii are larger than 1 R_J. The spread of values is dramatic around every mass within the range [0.17 M_J, 30 M_J], which emphasizes the strong sensitivity of ν_0 to planet parameters.

To investigate the crossed dependence of ν_0 on the radius and the planet mass, we calculate it for a wide range of radii and masses in the observed giant planet regime. Figure 6 portrays the corresponding results for $0.5 \leq M_P \leq 10\ M_J$, and $0.95 \leq R_P \leq 2.1\ R_J$. All the planet models are coreless, except for $R_P = 1.0\ R_J$. For this radius value, we calculate the function $\nu_0(M_P)$ for several core masses within the Jovian range $0 \leq M_{core} \leq 10\ M_\oplus$. We place the observed point for Jupiter, taken from Gaulme et al. (2011), at $M_P = 1.0\ M_J$. As can be seen, our model is consistent with the observational data. For any fixed value of the planet radius, it is clear that ν_0 is an increasing function of the planet mass M_P. However, the sensitivity of ν_0 to the planet mass decreases as the planet radius increases. In order to quantify this, we fit the curves of Figure 6 with straight lines, in the high-mass regime ($5 \leq M_P \leq 10\ M_J$), and calculate their derivatives. We find that, for a radius equal to 0.95 R_J, the corresponding derivative is 25 $\mu Hz\ M_J^{-1}$. At the extreme opposite end of the giant planet radius spectrum, for a radius equal to 2.1 R_J, the corresponding derivative is 8.0 $\mu Hz\ M_J^{-1}$.

We investigate the separate influence of the radius, the mass, and the core mass on giant exoplanet pulsation modes. We focus on one parameter at a time. We select three specific quantities to discuss this influence: the characteristic frequency ν_0, the eigenfrequencies of low-degree f-modes, and the eigenfrequencies of low-degree p-modes.

To determine the influence of planetary parameters on the characteristic frequency and on the frequency spectrum of exoplanets, we calculate these for a wide range of each parameter (radius, mass, entropy, and core mass), all other things being equal.

4.2. *Eigenfrequencies and characteristic frequencies of giant planets*

4.2.1. *Dependence on the planet mass*

We build several planetary models with the radius fixed at $R_P = 1.0\ R_J$ and with various masses. We use coreless models, since we are here exploring the dependence on mass. Table 7 presents various parameters of these models: the planet mass, M_P (in Jupiter units), the central pressure, p_c (in Mbars), the central density, ρ_c (in cgs units), the specific entropy, S (in $k_B/baryon$), and the characteristic frequency, ν_0 (in μHz). When the radius is fixed at 1.0 R_J, ν_0 is an increasing function of planet mass. We fit this function with a power law and obtain:

$$\nu_0(M_P) \sim 164.0 \times \left(\frac{M_P}{M_J}\right)^{0.48} \mu Hz\ . \qquad (9)$$

This dependence is due to the behavior of the the sound speed $c_0(r)$, which is linked to the frequency ν_0 by Equation 5. Figure 7 depicts the profiles of the pressure p_0 and the sound speed c_0 along the relative radius $x = r/R$, in hydrostatic equilibrium, for the first models of Table 7. As can be seen, at every level of the relative radius x, when the radius is fixed, both the pressure and the sound speed are increasing functions of the planet mass. Thus, given its definition (Eq. 5), ν_0 increases as the planet mass increases, all other things being equal.

According to the asymptotic theory, we know that, for a given low value of the degree l, and for large radial orders n, ν_0 is approximately the frequency gap between two modes of consecutive radial order: $\nu_{n+1,l} - \nu_{n,l} \sim \nu_0$. Thus, at high frequency, the spacing between eigenfrequencies increases when the planet mass increases, for a given value of the planet radius. Numerically, when the radius is fixed at $R_P = 1.0\ R_J$, for an object of 1.0 M_J, we know that the high-frequency modes are separated by $\sim$155 μHz, since this corresponds to the Jupiter case. For a 5.0-M_J planet, the frequency gap between high-frequency modes is $\sim$350 μHz, and, at the end of the giant planet regime, for a planet mass of 15.0 M_J, the frequency gap exceeds 500 μHz.

We now calculate the eigenfrequencies of the lowest-order p-modes for the objects defined in Table 7, and for $l \in [0, 8]$. Figure 8 presents the corresponding eigenvalues for n up to 12, as a function of the degree l, for objects with mass equal to 0.5, 1.0, 2.0, and 3.0 M_J, and a radius fixed at 1.0 R_J. The frequency spectra of the four planets appear more and more distinct from one another as we go up in frequency, and as we go up in degree l. Indeed, at low l, the f-modes of the four planets are close to one another, whereas the difference between the modes with the same n and l increases rapidly with frequency. Numerically, for $l = 2$, the f-modes of the four planets are all within the range $0.08 \leq \nu_{0,2} \leq 0.21$ mHz. For $l = 2$ and $n = 12$, the difference between the eigenvalues for $M_P = 0.5\ M_J$ and $M_P = 3.0\ M_J$ is more than 2.3 mHz. This discrepancy at high radial order n is, of course, due to the differences of the characteristic frequency ν_0, which is a measure of the frequency scale at low-degree l and high-order n. At high frequency, the value of ν_0 for each planet is clearly visible on Figure 8.

This increase of the frequency range continues as the planet mass increases beyond 3.0 M_J. To appreciate the difference numerically, we focus on $l \in [0, 8]$ and $n \in [0, 7]$. Figure 9 presents several low-order eigenvalues, as a function of the planet mass, for various values of the degree $l \in [0, 8]$. For the calculated modes, it appears from the calculations that the minimum in frequency is always obtained for $(n, l) = (0, 2)$ (middle left panel), and the maximum is obtained for the highest n and l considered: $(n, l) = (7, 8)$ (bottom right panel). This statement is true for every value of the planet mass M_P in the selected range. On the bottom right panel ($l = 8$), the functions $\nu_{0,2}(M_P)$ have been added (black dashed line). Thus, the frequency range of the calculated modes is contained between the black dashed line ($\nu_{0,2}$) and the solid gold line, defined by ($\nu_{7,8}$). Numerically, The low-degree, low-order eigenfrequencies of a 1.0-M_J planet are in the range [0.11,1.8] mHz, whereas the same eigenfrequencies of a 15-M_J object are in the range [0.50, 6.4] mHz.

4.2.2. *Dependence on the planet radius*

We build several planetary models with the mass fixed at $M_P = 1.0\ M_J$ and with various radii. Table 8 presents various parameters of these models: the planet radius, R_P (in Jupiter units), the central pressure, p_c (in Mbars), the central density, ρ_c (in cgs units), the specific entropy, S (in $k_B/baryon$), and the characteristic frequency, ν_0 (in μHz). When the mass is fixed at 1.0 M_J, ν_0 is a decreasing function of the planet radius. We again fit this function with a power law and obtain:

$$\nu_0(R_P) \sim 164.0 \times \left(\frac{R_P}{R_J}\right)^{-2.09} \mu Hz\ . \qquad (10)$$

If we compare Equations 9 and 10, we see that, for the selected ranges of values, the dependence of ν_0 on the radius is significantly more important than the dependence on the mass. As explained in the previous subsection, ν_0 is approximately the frequency gap between two modes of consecutive radial order, for a given low value of the degree l, and for large radial order n. Thus, this decreasing behavior results in a diminution of the frequency gap between high-frequency modes. Numerically, we can see that this gap is around 40 μHz for a 2.0-R_J planet (again, the mass is equal to 1.0 M_J), which is less than 26% of the Jovian value.

We calculate the eigenfrequencies of the lowest-order p-modes for the objects defined in Table 8, and for $l \in [0, 8]$. Figure 10 presents the corresponding eigenvalues for n up to 12, as a function of the degree l, for objects with a radius equal to 1.0, 1.2, 1.4 and 1.6 R_J, and a mass equal to 1.0 M_J. It appears that the remarks of the previous subsection, which deals with the dependence on the planet mass, also apply to Figure 10. Indeed, the frequency spectra of the four planet models appear more and more distinct from one another as we go up in frequency, and as we go up in degree l. The frequency range and scale of the low-degree, low-order eigenvalues decrease with the planet radius, when the mass is fixed, whereas the same parameters increase with the planet mass, when the radius is fixed. For instance, numerically, the low-degree, low-order eigenvalues of a 1.6-R_J planet are between 0.07 mHz and 0.91 mHz, whereas, in the case of a 1.0-R_J planet, the same modes have eigenfrequencies between 0.1 mHz and 2.6 mHz.

4.2.3. *Dependence on the core mass*

Even in the cases of Jupiter and Saturn, the presence and mass of a dense core is still not proven. Gudkova & Zarkhov (1999) have shown that measurements of the

pulsation modes of Jupiter could constrain the dimensions of the core. This is likely to be true for exoplanets, if and when their modes are measured. Many extrasolar giant planets appear smaller than the theory would allow (Burrows et al. 2007; Guillot et al. 2006). This anomaly can be explained by the presence of heavy elements in a dense core, which shrinks the radii of these planets. One famous example is the case of HD149026b, whose measured radius and mass suggest the presence of a core mass in the range 45 - 90 $M_\oplus$ (Sato et al. 2005).

We calculate the characteristic frequency ν_0 as a function of the core mass for a selection of exoplanets for which the presence of a core has been inferred. The results are given in Figure 11, which also includes the characteristic frequencies for Jupiter and Saturn, as a reference. The core mass ranges have been taken from Saumon & Guillot (2004) for Jupiter and Saturn, Sato et al. (2005) for HD149026b and Burrows et al. (2007) for the other planets. It is clear that, in any case, with the radius and the mass of the object fixed, ν_0 is a decreasing function of the core mass. This can be easily explained: the presence of a dense core reduces the sound speed in the center of the planet (see, for example, Figure 1) which ultimately increases the integral $\int_{planet} \frac{dr}{c}$ and, thus, diminishes ν_0, which is inversely proportionnal to the latter. However, the sensitivity to the mass of the core is not identical among the selected objects. We can see that Saturn and HD149026b are much more influenced by the core mass than the others. This is due to their small radius and mass, compared to the other selected planets. Indeed, Saturn's radius is 0.83 R_J, its mass is 0.30 M_J, HD149026b's radius is 0.72 R_J, its mass is 0.36 M_J whereas all the other planets have radii within the range [1.0,1.23] R_J and masses within the range [0.54,1.30] M_J. In this way, for planets with a small radius and mass, the determination of ν_0 through observation can be a powerful tool to investigate the presence of a dense core. For example, for our models of HD149026b, ν_0 loses more than 26% of its value between a 45-$M_\oplus$ core model and a 90-$M_\oplus$ core model. Thus, even a rough estimate of the value of ν_0 might give us information on the core of this type of planet.

To investigate the dependence of the low-degree, low-order eigenfrequencies on the core mass, we build several exoplanet models with the radius fixed at $R_P = 1.0\ R_J$, the mass fixed at $M_P = 1.0\ M_J$, and the core mass in the range 0-100 $M_\oplus$. Table 9 presents the various parameters of these models: the core mass, M_c (in Earth units), the central pressure, p_c (in Mbars), the central density, ρ_c (in cgs units), the specific entropy, S (in $k_B/baryon$), and the characteristic frequency, ν_0 (in μHz). The lowest-order eigenvalues of modal oscillations are given in Figure 12, as a function of the degree l, for models with a core mass equal to 0, 10, 20, 30, 50, and 100 $M_\oplus$, and with the radius and mass fixed at the Jovian values. When the radius and mass are fixed, the eigenfrequencies are monotonic functions of the core mass, but their direction of variation depends on their degree l and their radial order n. For $l \geq 2$, the eigenvalues of the f-modes increase when the core mass increases. At high n, for every l, it can be seen that the eigenfrequencies are decreasing functions of the core mass, all things being equal. For instance, numerically, between the coreless model and the model with a core mass fixed at 100 $M_\oplus$, the eigenvalues decrease by ∼15% at high n ($n \in [10, 12]$), for every $l \in [0, 8]$. Thus, for a given degree l, the f-modes and the high-order p-modes, as functions of the core mass, have opposite directions of variation. Consequently, the frequency range for a given l shrinks when the core mass increases. If the low-degree, low-order modes were to be unambiguously identified by its spherical harmonic quantum numbers, the corresponding frequency range may constrain the presence of heavy elements in the deep interior.

We have also constructed several exoplanet models with the mass fixed at $M_P = 1.0\ M_J$, and the specific entropy fixed at $S = 6.67\ k_B/baryon$, which is the specific entropy of our coreless model with $R_P = 1.0\ R_J$ and $M_P = 1.0\ M_J$. These models possess a core with a mass in the range 0-100 $M_\oplus$ and this set of planet models approximately probes the situation in which, for a given planet mass and a given age, the presence of a dense core shrinks the radius. Table 10 presents various parameters of these models: the core mass, M_c (in Earth units), the planet radius, R_P (in Jupiter units), the central pressure, p_c (in Mbars), the central density, ρ_c (in cgs units), and the characteristic frequency, ν_0 (in μHz). For the selected values of planet mass ($M_P = 1.0\ M_J$) and entropy ($S = 6.67\ k_B/baryon$), the shrinking of the radius with core mass is visible. For instance, the planet radius decreases by ∼20 % when a 100-$M_\oplus$ core is added. The direct consequence of the reduction of the radius is the increase of the characteristic frequency ν_0. Qualitatively, the increase of ν_0 is consistent with its dependence on the planet radius, discussed in section 4.2.2.

For the fixed radius and entropy, the eigenvalues of the lowest-order modal oscillations are given in Figure 12, as a function of the degree l, for models with a core mass equal to 0, 10, 20, 50, and 100 $M_\oplus$. When the mass and the entropy of the planet models are fixed, the frequency range of the low-degree, low-order p-modes decreases as the core mass increases. This is again a direct consequence of the shrinking of the planet radius as the core mass goes up, for given mass and entropy. However, as can be seen, the frequency spectra of the models defined by $M_c = 0\ M_\oplus$ and $M_c = 10\ M_\oplus$ are quite similar for $l \in [0, 3]$ and $n \in [0, 12]$. In particular, for $l = 1$ and 2, the eigenfrequencies of these two models differ by less than 1% for the frequency range considered. These similarities may be due to two opposite effects. First, we know that the presence of a 10-$M_\oplus$ dense core shrinks the model radius by 2% for the selected values of planet mass and entropy (see Table 10). When the planet mass is fixed, this decrease of the radius causes an increase of the low-degree, low-order eigenvalues, as already discussed in section 4.2.2. On the other hand, when the planet radius and the planet mass are both fixed, the presence of a dense core implies a decrease of the same eigenvalues. Figure 12 shows that, for the selected values, for low core mass and low degree l, the presence of a dense core compensates for the effect of the radius reduction on the eigenvalues. Nonetheless, it can be seen that, for higher degrees l ($l \geq 4$) and for higher core masses ($M_c \geq 20\ M_\oplus$), the effects of the radius reduction exceed the pure effect of the core.

4.2.4. *Dependence on the metallicity*

If not contained in a dense core, heavy elements can be laced throughout the envelope (Guillot 2005). In this spirit, we investigate the influence of heavy elements in the envelope itself, regardless of the presence of a core. Though there is no published robust equation of state that properly includes heavy elements beyond helium, we can mimic their presence by using a higher helium mass fraction than $Y = 0.25$ (Guillot 2008; Spiegel et al. 2011). We assume the excess of helium mass fraction ΔY (compared with the default value $Y_0 = 0.25$) is given by the value of the metallicity Z:

$$\Delta Y \sim Z \ . \tag{11}$$

Using the value from Asplund et al. (2009), we take $Z_\odot = 0.014$, to be the heavy element mass fraction in the Sun. In this way, an helium fraction of $Y = 0.30$ mimics a metallicity equal to $\sim$3.6 $\times$ solar metallicity.

We build three coreless models of exoplanets with a helium mass fraction of 0.25 and 0.30, respectively, with the radius and mass fixed at the Jovian values. The corresponding parameters, in particular the characteristic frequencies ν_0, are given in Table 11. As can be seen, a higher helium mass fraction, hence a higher fraction of heavy elements in the envelope, tends to lower the value of ν_0, all things being equal. Figure 14 portrays the low-degree, low-order eigenfreqdeuencies of the modal oscillations for the models of Table 11. It appears that the remarks made concerning Figure 12, which deals with the dependence on the core mass, can be also made for Figure 14. Such similarities are expected since, in both cases, it is the dependence on the global fraction of heavy elements that is under consideration. As can be seen on Figure 14, for low l and very low n, the eigenfrequencies slightly increase with the helium mass fraction Y, whereas for higher l and n, the eigenvalues unambiguously decrease with Y. As previously stated when discussing the presence of a dense core, if the low-degree, low-order modes were to be unambiguously identified, the corresponding frequency spectrum might give us a hint of the presence of heavy elements in the interior.

4.2.5. *Evolution of ν_0 with time*

To investigate the evolution of ν_0 for a given explanet, we build simple evolutionnary models of exoplanets with a mass fixed at 0.5, 1.0, 2.0, 10, and 20 M_J. We use the default formalism and modeling tools outlined in Burrows et al. (1997, 2001, 1995). The planets are in isolation, which means that no stellar irradiation is taken into account. No core has been added. As the specific entropy decreases with time, the planet's radius decreases. Figure 15 portrays the evolution of ν_0 and the planet radius up to 5 $Gyrs$ for the five fixed planet masses considered. The large early radii of the models result in small values for the characteristic frequencies, compared to their final values. Numerically, $\nu_0(0)$ is between 16% and 22% of the final ν_0 values, for the five models considered here. As the radius stabilizes, so does ν_0. We fit the curves with straight lines in the region [2,5] Gyrs, and we calculate the corresponding derivatives. We find that the derivative increases with the planet mass, from $\sim$3.1 $\mu Hz\ Gyrs^{-1}$ for $M_P = 0.5\ M_J$, to $\sim$8.2 $\mu Hz\ Gyrs^{-1}$ for $M_P = 20\ M_J$.

5. CONCLUSION

We have calculated the eigenfrequencies and eigenfunctions of the pulsational modes of planets for a broad range of giant exoplanet models. In particular, we have investigated the dependence of the characteristic frequency ν_0, the eigenfrequencies of low degree f-modes, and the eigenfrequencies of low degree p-modes on several parameters: the planet mass, the planet radius, the core mass, and the helium fraction in the envelope. We provide the corresponding eigenvalues for a degree l up to 8 and a radial order n up to 12. We also present values of ν_0 for 174 known giant exoplanets, and highlight the strong dependence on the radius, around any value of the planet mass.

For Jupiter and Saturn, we find that our results are consistent with both observationnal data (Gaulme et al. 2011) and previous theoretical work (Provost et al. 1993; Mosser et al. 1994; Gudkova & Zarkhov 1999). In the specific case of Jupiter, we presented ν_0 and the low-degree, low-order eigenfrequencies of acoustic modes as a function of the core mass. We conclude that, for non-radial oscillations ($l \geq 1$), the sensitivity of the pulsation frequencies to the core mass is important both for the f-modes and for the high-order p-modes. However, for specific intermediate values of radial order n, this sensitivity is minimal over the whole range of core masses considered.

Focusing on giant exoplanets, we find that the dependence of the characteristic frequency on the core mass is more important for small radii and masses. As an example, the characteristic frequency of HD149026b, with measured radius and mass of 0.72 R_J and 0.36 M_J, varies by more than 26% across the range of core masses considered. We quantify the influence of the core mass on exoplanet models with arbitrary fixed mass and radius. For $l \in [0, 8]$ and for frequencies up to 2.6 mHz, we find that eigenfrequencies shrink as the core mass increases, which is consistent with previous work on Jupiter. A big core ($M_c = 100\ M_\oplus$) induces a reduction in $\nu_{n,l}$ of $\sim$15% for $n \geq 10$ compared to coreless values. We also develop an approach to quantify the influence on the eigenfrequency spectrum of a high heavy-element fraction in the planet envelope. We find that, quantitatively, the presence of heavy element in the envelope affects the eigenvalue distribution in ways similar to the presence of a dense core.

We have also quantified the influence of mass and radius on the modal oscillations of giant exoplanets. For the selected values of l and n, we find that the pulsation eigenfrequencies depend strongly on both parameters, especially at high frequency. This dependence can be measured through ν_0. For the mass range $0.5 \leq M_P \leq 15\ M_J$, and fixing the planet radius to its Jovian value, we find that $\nu_0 \sim 164.0 \times (M_P/M_J)^{0.48}\ \mu Hz$. For the radius range from 0.9 to 2.0 R_J, and fixing the planet's mass to its Jovian value, we find that $\nu_0 \sim 164.0 \times (R_P/R_J)^{-2.09}\ \mu Hz$. These variations of ν_0 directly affect the high-frequency spectrum of modal oscillations.

We thank Dave Spiegel and Sudhir Raskutti for helpful discussions. The authors would also like to acknowledge support in part under HST grants HST-GO-12181.04-A, HST-GO-12314.03-A, and HST-GO-12550.02, and JPL/Spitzer Agreements 1417122, 1348668, 1371432,

1377197, and 1439064.

APPENDIX

NONRADIAL OSCILLATION EIGENVALUE PROBLEM

For adiabatic, nonradial oscillations of non rotating spherically symmetrical planetary models, the governing differential equations are (Unno et al. 1989, eqs. 14.2 - 14.4):

$$\frac{1}{r^2}\frac{d}{dr}\left(r^2\xi_r\right) - \frac{g}{c^2}\xi_r + \left(1 - \frac{L_l^2}{\sigma^2}\right)\frac{p'}{\rho c^2} = \frac{l(l+1)}{\sigma^2 r^2}\Phi', \tag{1}$$

$$\frac{1}{\rho}\frac{dp'}{dr} + \frac{g}{\rho c^2}p' + \left(N^2 - \sigma^2\right)\xi_r = -\frac{d\Phi'}{dr}, \tag{2}$$

and

$$\frac{1}{r^2}\frac{d}{dr}\left(r^2\frac{d\Phi'}{dr}\right) - \frac{l(l+1)}{r^2}\Phi' = 4\pi G\rho\left(\frac{p'}{\rho c^2} + \frac{N^2}{g}\xi_r\right), \tag{3}$$

where $c = (\Gamma p_0/\rho_0)^{1/2}$ is the sound speed and the Lamb frequency, L_l, is:

$$L_l^2 = \frac{l(l+1)c^2}{r^2} \tag{4}$$

and the Brunt-Väisälä frequency, N, is:

$$N^2 = g\left(\frac{1}{\Gamma}\frac{d\ln p_0}{dr} - \frac{d\ln\rho_0}{dr}\right). \tag{5}$$

$\Gamma = (d\ln p_0/d\ln\rho_0)_{ad}$ is the adiabatic exponent, G is the gravitation constant, $g = GM_r/r^2$ is the gravitational acceleration, and r is the radius. Primed variables refer to the Eulerian perturbation at a given position; zero subscripts refer to the equilibrium value.

Equations (1) - (3) are the full fourth-order set of differential equations. There are four corresponding boundary conditions (Unno et al. 1989, eqs. 14.8-14.11). At $r = 0$,

$$\xi_r - \frac{l}{\sigma^2 r}\left(\frac{p'}{\rho} + \Phi'\right) = 0 \tag{6}$$

and

$$\frac{d\Phi'}{dr} - \frac{l\Phi'}{r} = 0\ . \tag{7}$$

At $r = R$, where R is the radius of the planet,

$$\frac{d\Phi'}{dr} + \frac{l(l+1)}{r}\Phi' = 0 \tag{8}$$

and

$$\delta p = 0. \tag{9}$$

Here, δ is the Lagrangian perturbation for a given fluid element. Equation (9) has various limiting forms, depending on the physical conditions at $r = R$. For the case in which the density and pressure vanish at the surface, (9) can be written (Unno et al. 1989, eq. 14.12):

$$\xi_r - \frac{p'}{g\rho} = 0\ . \tag{10}$$

This condition is valid whenever

$$-\frac{d\ln p_0}{d\ln r} = \frac{r}{H} \gg 1 \tag{11}$$

at $r = R$. Thus, we need to estimate the pressure scale height, H, for every input model of the planet. As an example, Saturn's value is about 40 km at 1 bar (Marley 1990), making this condition for a free boundary appropriate. The differential equations, boundary conditions, and a normalization condition at $r = R$, $\xi_r/r = 1$, comprise the eigenvalue problem.

EIGENVALUE CALCULATION: THE DIMENSIONLESS PROBLEM

The eigenvalue differential equations (Eqs.1 - 3) may be recast as four first-order differential equations with four dimensionless variables (Unno et al. 1989). The variables are:

$$\begin{aligned} y_1 &= \frac{\xi_r}{r}, \\ y_2 &= \frac{1}{gr}\left(\frac{p'}{\rho} + \Phi'\right), \\ y_3 &= \frac{1}{gr}\Phi', \\ y_4 &= \frac{1}{g}\frac{d\Phi'}{dr}. \end{aligned} \tag{12}$$

The dimensionless variable

$$x = \frac{r}{R} \tag{13}$$

is used in place of r. The resulting four equations are as follows:

$$x\frac{dy_1}{dx} = (V_g - 3)\, y_1 + \left[\frac{l(l+1)}{c_1\omega^2} - V_g\right] y_2 + V_g y_3, \tag{14}$$

$$x\frac{dy_2}{dx} = \left(c_1\omega^2 - A^*\right) y_1 + (A^* - U + 1)\, y_2 + A^* y_3, \tag{15}$$

$$x\frac{dy_3}{dx} = (1 - U)\, y_3 + y_4, \tag{16}$$

and

$$x\frac{dy_4}{dx} = UA^* y_1 + UV_g y_2 + [l(l+1) - UV_g]\, y_3 + U y_4. \tag{17}$$

The dimensionless quantities are

$$V_g = \frac{d\ln M_r}{d\ln r} = \frac{gr}{c^2} \tag{18}$$

$$U = -\frac{1}{\Gamma}\frac{d\ln p}{d\ln r} = \frac{4\pi\rho r^3}{M_r} \tag{19}$$

$$c_1 = (r/R)\,/\,(M_r/M) \tag{20}$$

$$\omega^2 = \frac{\sigma^2 R^3}{GM} = \frac{4\pi^2\nu^2 R^3}{GM} \tag{21}$$

and

$$A^* = -rA = rg^{-1}N^2. \tag{22}$$

The dimensionless boundary conditions are

$$\frac{c_1\omega^2}{l} y_1 - y_2 = 0 \text{ at } r = 0 \tag{23}$$

$$l y_3 - y_4 = 0 \text{ at } r = 0 \tag{24}$$

$$(l+1) y_3 + y_4 = 0 \text{ at } r = R \tag{25}$$

$$y_1 - y_2 + y_3 = 0 \text{ at } r = R. \tag{26}$$

NUMERICAL IMPLEMENTATION

Using the previous equations and boundary conditions, we build two linearly independent solutions that satisfy the appropriate boundary conditions at the center and two linearly independent solutions that satisfy the appropriate boundary conditions at the surface. These solutions are carried out using a fifth-order Runge-Kutta method with adjusted stepsize to ensure accuracy. The solution vectors $\mathbf{y} = (y_i)$ are, respectively: $\mathbf{y}^{C,1}(x)$, $\mathbf{y}^{C,2}(x)$, $\mathbf{y}^{S,1}(x)$, and $\mathbf{y}^{S,2}(x)$, where the superscripts C and S denote a solution integrated from the center and the surface, respectively. A continuous match of the interior and exterior solutions at an arbitrary fitting point x_f requires the existence of non-zero constants $K_i^{C,1}$, $K_i^{C,2}$, $K_i^{S,1}$, and $K_i^{S,1}$, $i \in \{1, 2, 3, 4\}$ such that (Christensen-Dalsgaard 2003):

$$K_i^{C,1} y_i^{C,1}(x_f) + K_i^{C,2} y_i^{C,2}(x_f) = K_i^{S,1} y_i^{S,1}(x_f) + K_i^{S,2} y_i^{S,2}(x_f), \tag{27}$$

For all $i \in \{1, 2, 3, 4\}$. This set of equations has a solution only if the determinant

$$\Delta_f(\omega^2) = \left| \mathbf{y}^{C,1}(x_f) \quad \mathbf{y}^{C,2}(x_f) \quad \mathbf{y}^{S,1}(x_f) \quad \mathbf{y}^{S,2}(x_f) \right| \tag{28}$$

vanishes. Hence, the eigenfrequencies are determined as the zeros of $\Delta_f(\omega^2)$. This determinant has the advantage of behaving smoothly over the whole frequency spectrum and allows us to use a simple bisection method to find all the roots of Δ_f, while scanning a given interval of frequency.

The roots of Δ_f are supposed to be independent both of the choice of the fitting point and of the initial values of $\mathbf{y}^{C,1}$, $\mathbf{y}^{C,2}$, $\mathbf{y}^{S,1}$ and $\mathbf{y}^{S,2}$. However, it is possible to control the amplitude of the determinant by using the regular solutions near the center and the surface, given in Unno et al. 1989 and characterized by:

$$y_1 \sim x^{l-2} \qquad \text{for } r \sim 0, \tag{29}$$

$$y_1 \sim x^{-l} \qquad \text{for } r \sim R. \tag{30}$$

Thus, we define the following initial values for the center:

$$y_1^{C,1} = y_1^{C,2} = x^{l-2}, \tag{31}$$

$$y_3^{C,1} = f_1 \cdot y_1^{C,1}, \tag{32}$$

$$y_3^{C,2} = f_2 \cdot y_1^{C,1}, \tag{33}$$

and for the surface:

$$y_1^{S,1} = y_1^{S,2} = x^{l-2}, \tag{34}$$

$$y_3^{S,1} = g_1 \cdot y_1^{S,1}, \tag{35}$$

$$y_3^{S,2} = g_2 \cdot y_1^{S,1}, \tag{36}$$

where f_1, f_2, g_1 and g_2 are arbitrary coefficients such that $f_1 \neq f_2$ and $g_1 \neq g_2$. Then, for any particular frequency (actually ω^2), the values of $y_i^{C,j}$ and $y_i^{S,j}$ for $i = 2, 4$ and $j = 1, 2$ are fixed by the boundary conditions (23) - (26).

REFERENCES

Asplund, M., Grevesse, N., Sauval, J. A., & Scott, P. 2009, ARA&A, 47, 48
Bercovici, D. & Schubert, G. 1987, Icarus, 69, 557
Burrows, A., Saumon, D., Guillot, T., Hubbard, W. B., & Lunine, J. L. 1995, Nature, 375, 299
Burrows, A., Marley, M., Hubbard, W. B. et al. 1997, ApJ, 491, 856
Burrows, A., Hubbard, W. B., Lunine, J. L., & Liebert, J. 2001, RMP, 73,719
Burrows, A., Hubeny, I., Budaj, J., & Hubbard, W., B. 2007, ApJ, 661, 502
Cox, J. P. 1976, A&A, 14, 247
Cox, J. P. 1980, Princeton University Press
Charbonneau, D., Brown, T. M., Noyes, R., W., & Gilligand R.,L. 2002, ApJ, 558, 377
Christensen-Dalsgaard, J. 1997, Institut for Fysik og Astronomi
Christensen-Dalsgaard, J. 2003, Lecture notes (5^{th} edition), Institut for Fysik og Astronomi
Christensen-Dalsgaard, J., Mullan, D.J. 1994, MNRAS, 270, 921
Dodson-Robinson, S. E., Bondenheimer, P. 2009, ApJ, 695, L159
Gaulme, P., Schmider, F.X., Gay, J., Guillot, T., & Jacob, C. 2011, A&A, 531, 104
Gudkova, T., Mosser, B., Provost, J., Chabrier, G., Gautier, D., & Guillot, T. 1995, A&A, 303, 594
Gudkova, T. & Zharkov, V.N. 1999, Planet. Space Sci., 47, 1211
Guillot, T. 1999, Planet. Space Sci., 47, 1183
Guillot, T. 2005, Annu. Rev. Earth Planet. Sci., 33
Guillot, T., Santos, N. C., Pont, F., Iro, N., Melo, C., & Ribas, I. 2006, A&A, 453, L21
Guillot, T. 2008, Physica Scripta Volume T, 130, 014023
Hubbard, W. R. & Marley, M. S. 1989, Icarus, 78, 102
Leconte, J., Baraffe, I., Chabrier, G., Barman, T., & Levrard, B. 2009, A&A, 506, 385
Lee, U. 1993, ApJ, 405, 359
Marley, M. S. 1990, Ph.D. Thesis, University of Arizona
Mosser, B., Schmider, F., X., Delache, Ph., & Gautier, D. 1991, A&A, 251, 356
Mosser, B., Mekarnia, D., Maillard, J., P., Gay, J., Gautier, D., & Delache, Ph. 1993, A&A, 267, 604
Mosser, B., Gudkova, & T., Guillot, T. 1994, A&A, 291, 1019
Mosser, B., Maillard, J., P., & Mekarnia, D. 2000, Icarus, 144, 104
Pollack, J.B., Hubickyj, O., Bodenheimer, & P., Lissauer, J.J. 1996, Icarus, 124, 62
Provost, J., Mosser, B., & Berthomieu, G. 1993, A&A, 274, 595
Robe, H. 1968, An. Ap., 31, 475
Saio, H. 1993, Ap&SS, 210, 61
Saumon, D., Hubbard, W. B., Burrows, A., Guillot, T., Lunine, J. I., & Chabrier, G. 1996, ApJ, 460, 993
Saumon, D. & Guillot, T. 2004, ApJ, 609, 1170
Saumon, D., Chabrier, G., & Van Horn, H.M. 1995, ApJ, 99, 713
Sato, B. et al. 2005, ApJ, 633, 465
Schmider, F.-X., Mosser, B., & Fossat, E. 1991, A&A, 248, 281
Schneider, J., Dedieu, C., Le Sidaner, P., Savalle, R., & Zolotukhin, I. 2011, A&A, 532, A79
Spiegel, D. S., Burrows, A., & Milsom, J. A. 2011, ApJ, 727, 57
Takata, M. & Löfller, W. 2004, PASP, 310
Udry, S. & Santos, N. C. 2007, ARA&A, 45, 397
Unno, W., Osaki, Y., Ando, H., Saio, H., & Shibahashi, H. 1989, University of Tokyo Press
Vidal-Madjar, A., Lecavelier des Etangs, A., Desert, J.-M., Ballester, G. E. et al. 2003, Nature, 422, 143
Vorontsov, S.V., Zharkov, V.N., & Lubimov, V.M. 1976, Icarus, 27, 109
Vorontsov, S.V., 1981 AZh, 58, 1275
Vorontsov & S.V., Zharkov 1981, AZh, 58, 1101
Vorontsov & S.V., Zharkov 1981, Usp. Fiz. Nauk., 134, 1675
Vorontsov, S.V., Gukdova, T.V., & Zharkov, V.N. 1989, Soviet Ast., 15
Winn, J. N. et al. 2008, ApJ, 675, 1531

TABLE 1
EIGENFREQUENCIES OF P-MODES OF DEGREE 0 AND 1 FOR A POLYTROPE OF INDEX 3, IN μHz.THE RADIUS IS $R_P = 6.9599 \times 10^{10}\ cm$ AND THE MASS IS $M_P = 1.989 \times 10^{33}\ g$.

l	0		1	
n	This work	CDM*	This work	CDM*
1	303.7754	303.7755	337.2152	337.2152
2	411.5268	411.5269	463.5716	463.5718
3	532.9179	532.9181	590.0692	590.0694
4	658.1677	658.1679	716.6286	716.6289
5	784.3664	784.3667	843.1062	843.1066
6	910.7238	910.7242	969.4328	969.4331
7	1036.9925	1036.9929	1095.5829	1095.5832
8	1163.0917	1163.0922	1221.5526	1221.5530
9	1289.0005	1289.0010	1347.3477	1347.3484
10	1414.7209	1414.7214	1472.9793	1472.9799
11	1540.2639	1540.2645	1598.4587	1598.4594
12	1665.6437	1665.6443	1723.7983	1723.7990
13	1790.8749	1790.8756	1849.0098	1849.0105
14	1915.9720	1915.9728	1974.1042	1974.1051
15	2040.9483	2040.9489	2099.0918	2099.0928
16	2165.8149	2165.8160	2223.9823	2223.9831
17	2290.5839	2290.5848	2348.7834	2348.7844
18	2415.2641	2415.2651	2473.5035	2473.5043
19	2539.8643	2539.8653	2598.1491	2598.1500
20	2664.3924	2664.3933	2722.7266	2722.7276
21	2788.8549	2788.8558	2847.2419	2847.2430
22	2913.2577	2913.2588	2971.6997	2971.7011
23	3037.6068	3037.6078	3096.1059	3096.1067
24	3161.9068	3161.9076	3220.4627	3220.4639
25	3286.1614	3286.1626	3344.7754	3344.7767

REFERENCES. — *Christensen-Dalsgaard & Mullan (1994, Table 2).

TABLE 2
EIGENFREQUENCIES OF P-MODES OF DEGREE 2 AND 3 FOR A POLYTROPE OF INDEX 3, IN μHz. THE RADIUS IS $R_P = 6.9599 \times 10^{10}\ cm$ AND THE MASS IS $M_P = 1.989 \times 10^{33}\ g$.

l	2		3	
n	This work	CDM*	This work	CDM*
1	390.1222	390.1223	428.8390	428.8391
2	516.1991	516.1992	558.2978	558.2981
3	643.0675	643.0677	686.8728	686.8732
4	769.7799	769.7802	814.7025	814.7027
5	896.2907	896.2910	942.0263	942.0267
6	1022.6131	1022.6135	1068.9862	1068.9866
7	1148.7618	1148.7622	1195.6634	1195.6639
8	1274.7484	1274.7491	1322.1083	1322.1090
9	1400.5845	1400.5849	1448.3544	1448.3552
10	1526.2791	1526.2795	1574.4258	1574.4265
11	1651.8419	1651.8424	1700.3401	1700.3411
12	1777.2824	1777.2825	1826.1125	1826.1136
13	1902.6072	1902.6082	1951.7557	1951.7561
14	2027.8269	2027.8277	2077.2784	2077.2793
15	2152.9475	2152.9485	2202.6912	2202.6923
16	2277.9762	2277.9776	2328.0025	2328.0032
17	2402.9209	2402.9216	2453.2187	2453.2197
18	2527.7854	2527.7867	2578.3473	2578.3482
19	2652.5775	2652.5785	2703.3935	2703.3949
20	2777.3017	2777.3023	2828.3646	2828.3655
21	2901.9614	2901.9629	2953.2632	2953.2651
22	3026.5636	3026.5648	3078.0968	3078.0983
23	3151.1104	3151.1121	3202.8689	3202.8695
24	3275.6070	3275.6085	3327.5814	3327.5828
25	3400.0566	3400.0577	3452.2396	3452.2418

REFERENCES. — * Christensen-Dalsgaard & Mullan (1994, Table 2).

TABLE 3
EIGENFREQUENCIES OF G-MODES FOR A POLYTROPE OF INDEX 3, IN μHz. THE RADIUS IS $R_P = 6.9599 \times 10^{10}\ cm$ AND THE MASS IS $M_P = 1.989 \times 10^{33}\ g$.

l	2		3	
n	This work	CDM*	This work	CDM*
-20	31.1798	31.1797	43.0341	43.0356
-19	32.6437	32.6439	45.0003	45.0009
-18	34.2535	34.2535	47.1556	47.1552
-17	36.0311	36.0313	49.5267	49.5272
-16	38.0054	38.0053	52.1528	52.1519
-15	40.2096	40.2099	55.0737	55.0718
-14	42.6886	42.6884	58.3407	58.3400
-13	45.4951	45.4953	62.0230	62.0230
-12	48.7014	48.7010	66.2057	66.2053
-11	52.3970	52.3972	70.9964	70.9960
-10	56.7061	56.7065	76.5390	76.5389
-9	61.7959	61.7959	83.0266	83.0267
-8	67.8987	67.8991	90.7245	90.7243
-7	75.3534	75.3535	100.0041	100.0058
-6	84.6648	84.6649	111.4182	111.4181
-5	96.6263	96.6264	125.7916	125.7915
-4	112.5543	112.5543	144.4538	144.4530
-3	134.7963	134.7963	169.6560	169.6563
-2	167.9278	167.9279	205.5287	205.5286
-1	221.3677	221.3677	259.7578	259.7578

REFERENCES. — * Christensen-Dalsgaard & Mullan (1994, Table 4).

TABLE 4
PARAMETERS OF THE MODELS OF JUPITER (J) AND SATURN (S).

Model	Y	$M_{core}\ (M_\oplus)$	$p_c\ (Mbars)$	$\rho_c\ (g\ cm^{-3})$	$\nu_0\ (\mu Hz)$
J1	0.25	0.0	39.2	4.14	157.4
J2	0.30	0.0	41.7	4.25	153.0
J3	0.25	5.0	71.6	19.4	152.4
J4	0.25	10.0	96.1	21.8	151.2
S1	0.25	13.0	44.2	16.1	118.6
S2	0.25	18.1	59.8	18.1	115.0
S3	0.30	18.1	60.7	18.2	112.2

TABLE 5
PERIODS OF P-MODES FOR THE J4 MODEL (IN MIN).

l						
n	0	1	2	3	4	5
0	-	-	138.38	101.18	84.49	74.46
1	104.31	59.44	48.07	41.52	37.11	33.93
2	45.53	34.19	30.13	27.41	25.42	23.89
3	30.61	24.93	22.74	21.21	20.00	19.00
4	23.50	20.08	18.55	17.46	16.60	15.88
5	19.24	16.92	15.75	14.94	14.26	13.69

TABLE 6
Characteristic frequency ν_0 (in μHz) for a set of coreless models using the estimated radius and mass (here in Jupiter units) of detected giant exoplanets.

Planet	R_{planet} (R_J)	M_{planet} (M_J)	ν_0 (μHz)
Kepler-9c	0.823	0.171	94.40
HAT-P-18b	0.995	0.197	65.01
HAT-P-12b	0.959	0.211	73.14
Kepler-34b	0.764	0.220	149.0
WASP-29b	0.792	0.244	141.9
Kepler-9b	0.842	0.252	114.1
HAT-P-38b	0.825	0.267	129.8
WASP-39b	1.270	0.280	47.87
HAT-P-19b	1.132	0.292	61.16
WASP-20b	0.900	0.300	105.4
WASP-21b	1.210	0.300	54.29
WASP-69b	1.000	0.300	80.85
HD-149026b	0.718	0.356	229.4
WASP-49b	1.115	0.378	72.11
WASP-63b	1.430	0.380	44.52
WASP-67b	1.400	0.420	48.45
Kepler-12b	1.695	0.431	35.07
Kepler-7b	1.614	0.433	38.18
WASP-11b	1.045	0.460	92.36
CoRoT-5b	1.388	0.467	51.76
WASP-31b	1.537	0.478	43.59
WASP-13b	1.365	0.485	54.39
WASP-17b	1.991	0.486	33.51
WASP-60b	0.900	0.500	143.5
WASP-42b	1.080	0.500	89.56
WASP-52b	1.300	0.500	60.66
WASP-6b	1.224	0.503	68.68
KOI-254b	0.960	0.505	120.4
HAT-P-1b	1.217	0.524	70.94
HAT-P-17b	1.010	0.534	108.5
CoRoT-16b	1.170	0.535	77.76
OGLE-TR-111b	1.077	0.540	93.89
WASP-15b	1.428	0.542	52.87
HAT-P-25b	1.190	0.567	77.34
WASP-62b	1.390	0.570	56.96
WASP-55b	1.300	0.570	64.76
WASP-25b	1.260	0.580	69.56
WASP-22b	1.158	0.588	83.46
WASP-34b	1.220	0.590	74.97
WASP-56b	1.200	0.600	78.27
WASP-54b	1.400	0.600	57.66
Kepler-8b	1.419	0.603	56.37
XO-2b	0.973	0.620	130.3
HAT-P-28b	1.212	0.626	78.36
Kepler-15b	0.960	0.660	139.9
HAT-P-27b	1.055	0.660	109.8
Kepler-6b	1.323	0.669	67.80
HAT-P-9b	1.400	0.670	60.92
OGLE-TR-10b	1.720	0.680	42.53
HAT-P-4b	1.270	0.680	74.19
HAT-P-24b	1.242	0.685	77.99
WASP-59b	0.900	0.700	181.6
HAT-P-30b	1.340	0.711	68.21
HD-209458b	1.380	0.714	64.62
WASP-35b	1.320	0.720	70.67
CoRoT-4b	1.190	0.720	87.62
OGLE-TR-211b	1.260	0.750	79.26
TrES-1	1.099	0.761	107.7
HAT-P-33b	1.827	0.763	40.7
HAT-P-29b	1.107	0.778	107.1
WASP-68b	0.900	0.800	196.7
WASP-57b	1.100	0.800	110.3
CoRoT-9b	1.050	0.840	126.6
WASP-2b	1.079	0.847	119.2
HAT-P-13b	1.280	0.850	81.77
WASP-16b	1.008	0.855	141.4
WASP-1b	1.484	0.860	61.93
KOI-202b	1.020	0.880	139.4
WASP-23b	0.962	0.884	163.6
WASP-44b	1.140	0.889	107.5
WASP-79b	1.700	0.890	49.60
XO-1b	1.184	0.900	99.52
WASP-28b	1.120	0.910	113.3
TrES-4	1.706	0.917	50.07

Note. — The helium mass fraction has been fixed at 0.25 in the entire envelope. No core has been added. Estimated radii

TABLE 6
Characteristic frequency ν_0 (in μHz) for a set of coreless models using the estimated radius and mass (here in Jupiter units) of detected giant exoplanets

Planet	R_{planet} (R_J)	M_{planet} (M_J)	ν_0 (μHz)
CoRoT-12b	1.440	0.917	67.65
WASP-41b	1.210	0.920	95.95
HAT-P-32b	2.037	0.941	44.39
WASP-7b	1.330	0.960	80.61
WASP-48b	1.670	0.980	53.73
WASP-45b	1.160	1.007	110.4
KOI-204b	1.240	1.020	95.95
WASP-26b	1.281	1.028	90.00
CoRoT-1b	1.490	1.030	67.42
WASP-24b	1.104	1.032	125.3
HAT-P-35b	1.332	1.054	84.32
HAT-P-6b	1.330	1.057	84.70
OGLE-TR-182b	1.470	1.060	70.14
HAT-P-5b	1.252	1.060	95.89
Qatar-1b	1.164	1.090	114.2
WASP-58b	1.300	1.100	90.49
CoRoT-19b	1.450	1.110	73.68
WASP-4b	1.363	1.121	83.28
HD-189733b	1.138	1.138	122.9
WASP-47b	1.150	1.140	120.2
WASP-78b	1.750	1.160	54.10
WASP-19b	1.386	1.168	82.39
HAT-P-37b	1.178	1.169	115.3
OGLE-TR-132b	1.230	1.170	104.8
OGLE-TR-113b	1.110	1.240	136.2
TrES-2	1.169	1.253	121.6
OGLE-TR-56b	1.200	1.300	116.9
CoRoT-13b	0.885	1.308	562.3
HAT-P-8b	1.500	1.340	76.46
WASP-12b	1.736	1.404	60.61
WASP-50b	1.153	1.468	136.3
KELT-2Ab	1.306	1.486	104.9
WASP-65b	1.300	1.600	110.1
WASP-5b	1.171	1.637	139.2
WASP-37b	1.136	1.696	151.9
TrES-5	1.209	1.778	135.3
HAT-P-7b	1.421	1.800	98.83
HAT-P-36b	1.264	1.832	125.2
HATS-1b	1.302	1.855	118.8
TrES-3	1.305	1.910	120.1
HAT-P-15b	1.072	1.946	187.1
WASP-43b	1.036	2.034	207.8
WASP-61b	1.240	2.060	138.6
WASP-3b	1.454	2.060	101.8
HAT-P-23b	1.368	2.090	115.0
WASP-46b	1.310	2.101	125.4
Kepler-5b	1.431	2.114	106.3
HAT-P-22b	1.080	2.147	193.1
HAT-P-31b	1.070	2.171	198.6
HAT-P-14b	1.200	2.200	153.7
KOI-428b	1.170	2.200	162.5
WASP-8b	1.038	2.244	217.3
CoRoT-21b	1.300	2.260	132.4
WASP-36b	1.269	2.279	139.5
WASP-66b	1.390	2.320	118.0
CoRoT-17b	1.020	2.450	236.9
Kepler-17b	1.312	2.450	135.8
Qatar-2b	1.144	2.487	182.0
CoRoT-11b	1.390	2.490	122.7
WASP-53b	1.200	2.500	164.3
WASP-38b	1.079	2.712	217.4
CoRoT-10b	0.970	2.750	285.3
CoRoT-23b	1.050	2.800	235.6
CoRoT-6b	1.166	2.960	190.6
WASP-10b	1.080	3.060	230.1
HD-17156b	1.095	3.191	227.5
KOI-135b	1.200	3.230	187.6
CoRoT-2b	1.465	3.310	129.9
HAT-P-34b	1.107	3.328	226.6
CoRoT-18b	1.310	3.470	163.9
WASP-32b	1.180	3.600	205.3
HD-80606b	0.921	3.940	380.3
HAT-P-21b	1.024	4.063	297.8
HAT-P-16b	1.289	4.193	186.6

Note. — The helium mass fraction has been fixed at 0.25 in the entire envelope. No core has been added. Estimated radii

TABLE 6
Characteristic frequency ν_0 (in μHz) for a set of coreless models using the estimated radius and mass (here in Jupiter units) of detected giant exoplanets

Planet	R_{planet} (R_J)	M_{planet} (M_J)	ν_0 (μHz)
OGLE2-TR-L9b	1.614	4.340	126.5
WASP-33b	1.438	4.590	160.1
HR-8799b	1.100	7.000	328.2
WASP-14b	1.281	7.341	252.4
CoRoT-14b	1.090	7.600	347.5
KOI-13b	1.830	8.300	158.2
Kepler-14b	1.136	8.400	336.8
HAT-P-2b	0.951	8.740	490.3
Kepler-30c	1.290	9.100	278.3
SWEEPS-11	1.130	9.700	364.8
HR-8799c	1.300	10.000	288.1
HR-8799d	1.200	10.000	332.0
WASP-18b	1.165	10.430	357.5
1RXS1609b	1.700	14.000	216.3
HN-Pegb	1.100	16.000	487.6
Kepler-30d	0.960	17.000	639.1
KOI-423b	1.220	18.000	432.3
2M-2140+16b	0.920	20.000	742.3
GQ-Lupb	1.800	21.500	264.3
CoRoT-3b	1.010	21.660	653.3
2M-2206-20b	1.300	30.000	501.3
2M-0746+20b	0.970	30.000	815.6

Note. — The helium mass fraction has been fixed at 0.25 in the entire envelope. No core has been added. Estimated radii and masses have been taken from *http://www.exoplanet.eu*

TABLE 7
PARAMETERS OF CORELESS EXOPLANET MODELS OF VARIOUS MASSES WITH A RADIUS FIXED AT $R_P = 1.0\ R_J$. THE HELIUM MASS FRACTION IN THE ENVELOPE IS 0.25.

$M_P\ (M_J)$	$p_c\ (Mbar)$	$\rho_c\ (g\ cm^{-3})$	Specific entropy $S\ (k_B/baryon)$	$\nu_0\ (\mu Hz)$
0.5	9.8	2.0	6.9	107.3
1.0	39.2	4.1	6.7	157.4
2.0	162.5	8.6	6.5	225.8
3.0	383.8	13.6	6.6	274.3
5.0	1176	24.7	7.1	345.4
10.0	5612	55.8	8.2	467.2
15.0	14075	89.1	8.9	560.5

TABLE 8
PARAMETERS OF CORELESS EXOPLANET MODELS FOR VARIOUS RADII WITH A MASS FIXED AR $M_P = 1.0\ M_J$. THE HELIUM MASS FRACTION IN THE ENVELOPE IS 0.25.

$R_P\ (R_J)$	$p_c\ (Mbar)$	$\rho_c\ (g\ cm^{-3})$	Specific entropy $S\ (k_B/baryon)$	$\nu_0\ (\mu Hz)$
0.9	48.2	5.0	3.5	220.2
1.0	39.2	4.1	6.7	157.4
1.2	28.7	3.0	8.7	102.0
1.4	22.5	2.3	9.7	74.57
1.6	17.9	1.8	10.3	58.47
1.8	14.2	1.5	10.7	47.78
2.0	11.5	1.2	10.9	40.08

TABLE 9
PARAMETERS OF EXOPLANET MODELS FOR VARIOUS CORE MASSES M_c WITH A PLANET MASS FIXED AT $M_P = 1.0\ M_J$ AND A PLANET RADIUS FIXED AT $R_P = 1.0\ R_J$. THE HELIUM MASS FRACTION IN THE ENVELOPE IS 0.25.

$M_c\ (M_\oplus)$	$p_c\ (Mbar)$	$\rho_c\ (g\ cm^{-3})$	Specific entropy $S\ (k_B/baryon)$	$\nu_0\ (\mu Hz)$
0	39.2	4.1	6.7	157.4
10	96.9	21.8	7.0	151.2
20	145.7	25.8	7.3	149.4
30	198.9	29.2	7.6	147.5
50	307.9	35.5	8.1	143.0
100	645.4	49.5	9.2	134.1

TABLE 10
PARAMETERS OF EXOPLANET MODELS FOR VARIOUS CORE MASSES M_c WITH A PLANET MASS FIXED AT $M_P = 1.0\ M_J$ AND A SPECIFIC ENTROPY FIXED TO 6.67 $k_B/baryon$ (VALUE FOR A CORELESS MODEL WITH $R_P = 1.0\ R_J$ AND $M_P = 1.0\ M_J$). THE HELIUM MASS FRACTION IN THE ENVELOPE IS 0.25.

$M_c\ (M_\oplus)$	$R_P\ (R_J)$	$p_c\ (Mbar)$	$\rho_c\ (g\ cm^{-3})$	$\nu_0\ (\mu Hz)$
0	1.0	39.2	4.1	157.4
10	0.98	100.1	23.0	160.0
20	0.96	152.2	27.3	166.8
30	0.94	209.1	31.2	173.0
50	0.90	329.5	38.1	187.3
100	0.81	680.6	53.0	223.6

TABLE 11
Parameters of coreless exoplanet models for some helium mass fraction Y in the envelope with a planet mass fixed at $M_P = 1.0\ M_J$ and a planet radius fixed at $R_P = 1.0\ R_J$.

Y	$p_c\ (Mbar)$	$\rho_c\ (g\ cm^{-3})$	Specific entropy $S\ (k_B/baryon)$	$\nu_0\ (\mu Hz)$
0.25	39.2	4.1	6.7	157.4
0.30	41.7	4.3	6.9	153.12

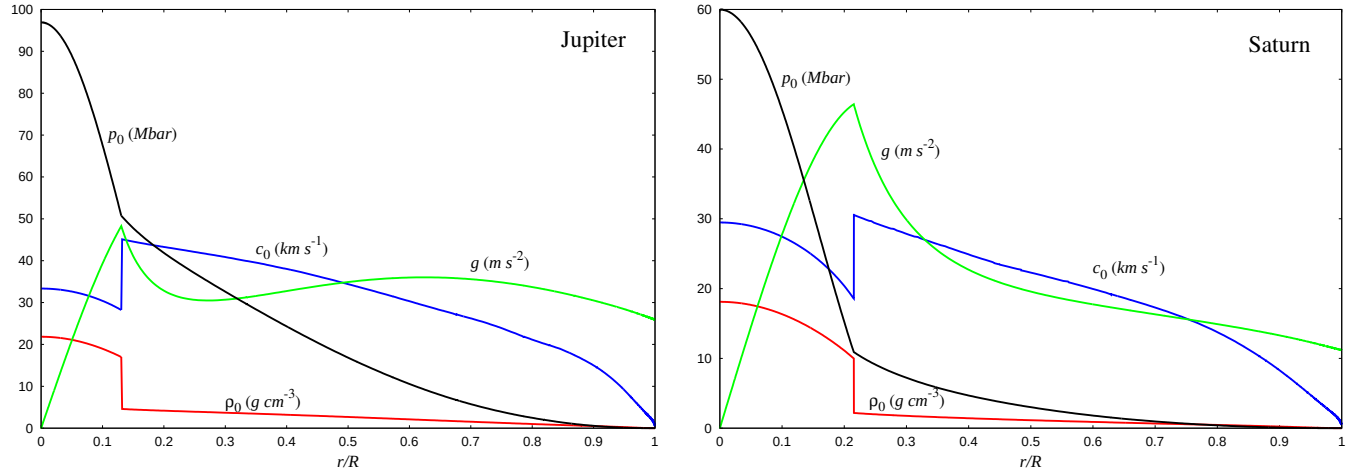

FIG. 1.— Left panel: Distribution of density ρ_0 ($g\ cm^{-3}$), gravitational acceleration g ($cm\ s^{-2}$), pressure p_0 ($Mbar$), and sound speed c_0 ($km\ s^{-1}$) as a function of the relative radius r/R for the model J4 of Jupiter. Right panel: The same in the case of the model S2 of Saturn. One has to notice that the scales of the Y-axis are different on the two figures.

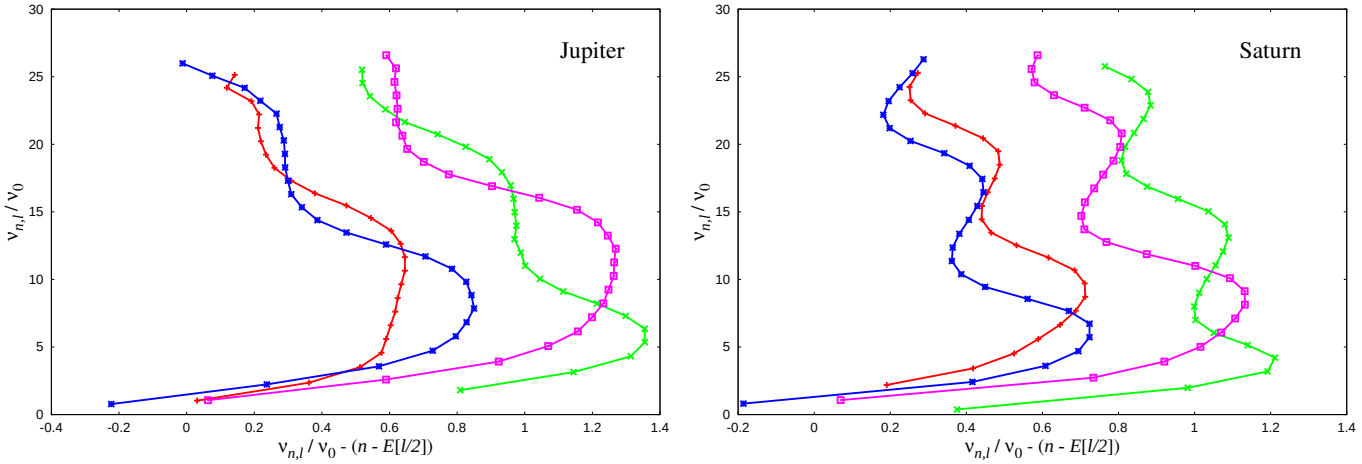

FIG. 2.— Left panel: Echelle diagrams of the eigenfrequencies of Jupiter (model J4) for $l \in [0,3]$ and $n \in [0,25]$. The characteristic frequency, ν_0, is 151.2 μHz ($l = 0$: $+$, $l = 1$: $\times$, $l = 2$: $*$, $l = 3$: $\boxdot$). Right panel: The same in the case of the model S2 of Saturn. The characteristic frequency, ν_0, is 115.0 μHz.

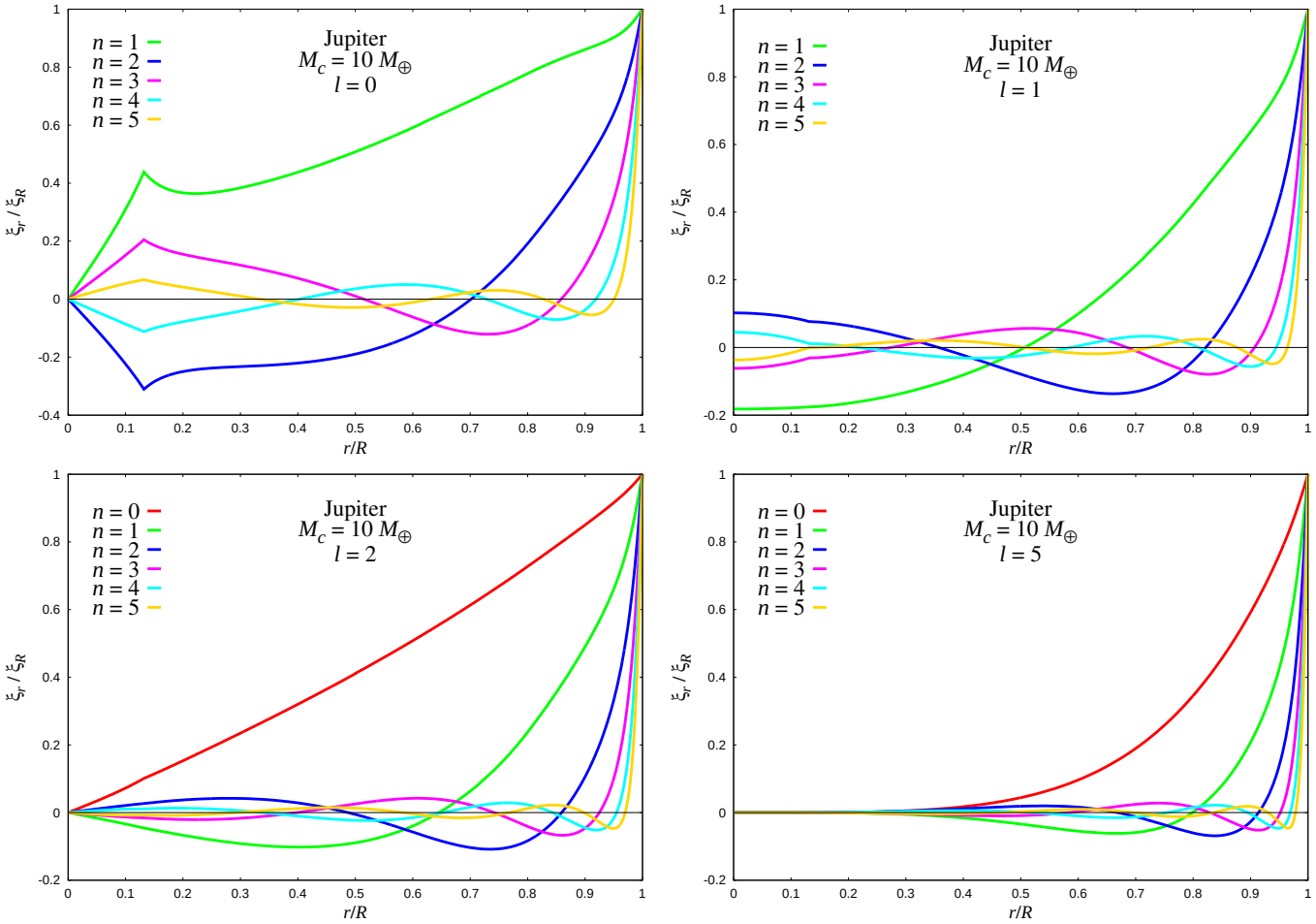

FIG. 3.— Radial component of the eigendisplacement ξ_r for low-degree, lowest-order modal oscillations of the model J4 of Jupiter, which has a core mass equal to $M_c = 10 M_\oplus$. The radial displacement is taken equal to 1 m at the surface; in other words, the radial displacement ξ_r is normalized by its value ξ_R at the surface. Top left: $l = 0$; top right: $l = 1$; bottom left: $l = 2$; bottom right: $l = 5$.

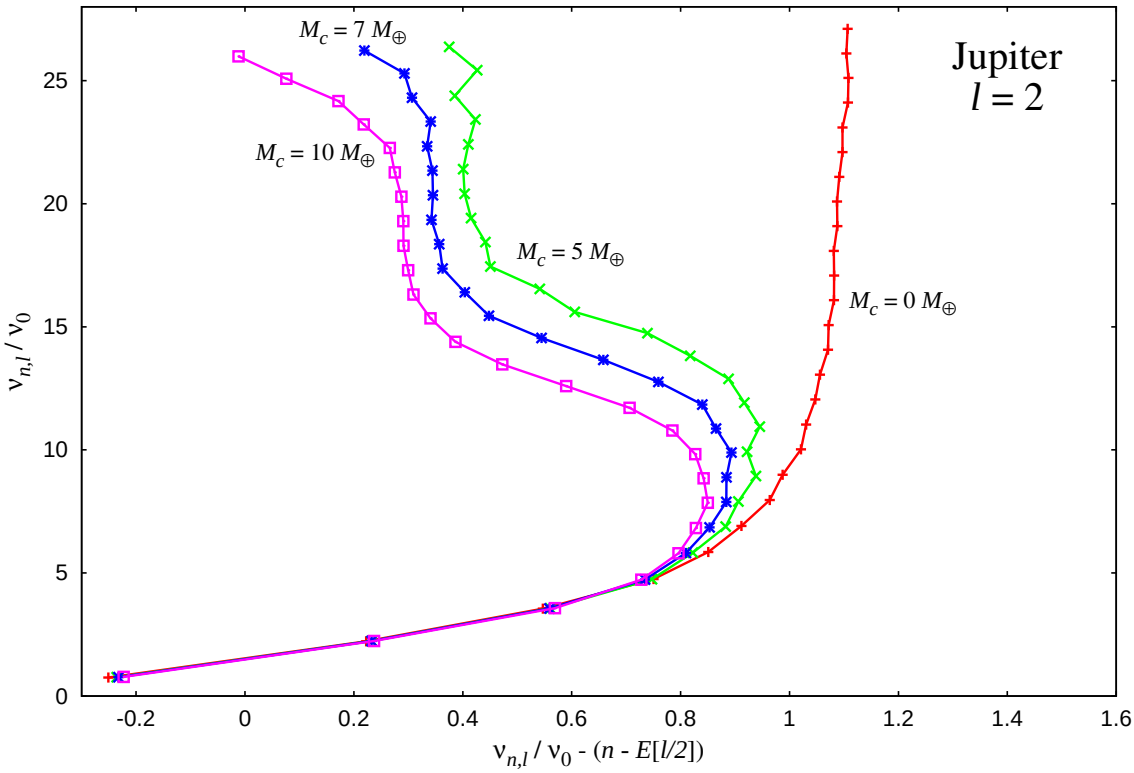

FIG. 4.— Echelle diagrams of the Jovian eigenfrequencies calculated for different core masses with $\nu_0 = 155\ \mu Hz$ and $l = 2$ (In Earth units, the corresponding core masses are $M_{core} = 0$: $+$, $M_{core} = 5$: $\times$, $M_{core} = 7$: $*$, $M_{core} = 10$: $\boxdot$).

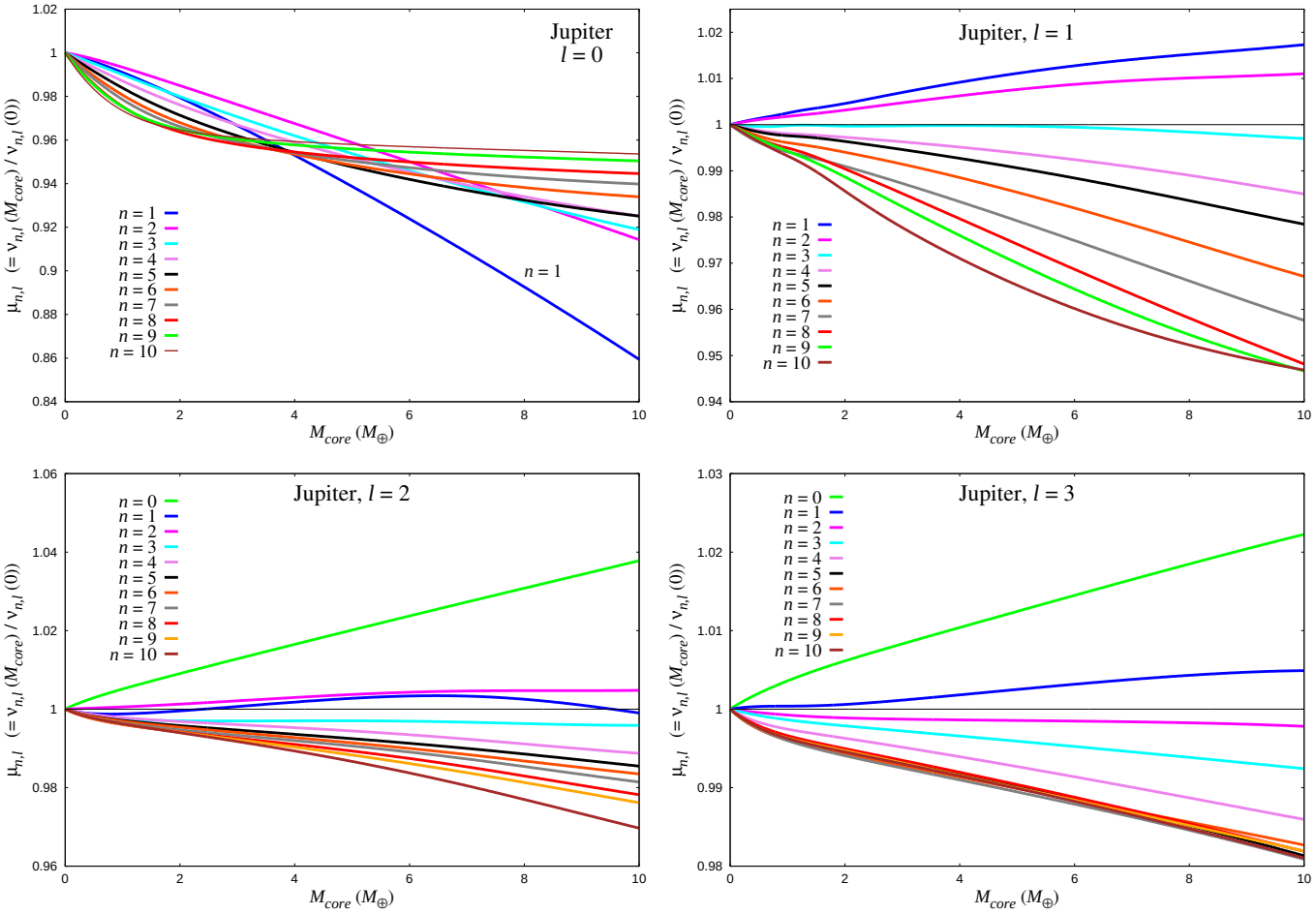

FIG. 5.— Top left panel: Eigenfrequencies of p-modes for Jupiter as a function of the core mass for $l = 0$. For every radial order n, the eigenfrequencies have been normalized by their coreless value: $\mu_{n,l}(M_{core}) = \nu_{n,l}(M_{core})/\nu_{n,l}(0)$. We assume that $0 \leq M_{core} \leq 10 M_{\oplus}$. Top right panel: same as for the top left panel, but for $l = 1$. Bottom left panel: same as for the top left panel, but for $l = 2$. Bottom right panel: same as for the top left panel, but for $l = 3$.

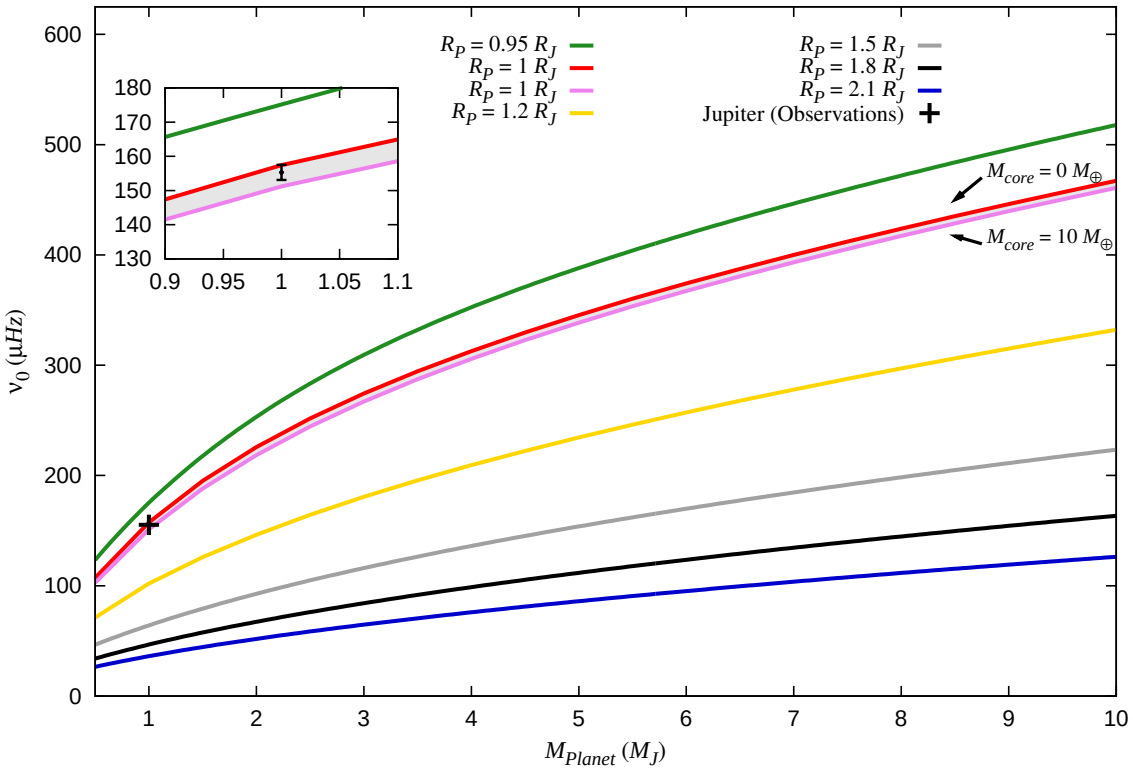

FIG. 6.— The charateristic frequency, ν_0, as a function of the planet mass, for various planet radii. The helium mass fraction in the envelope has been set to 0.25. The models are all coreless except for $R_P = 1.0\ R_J$. For this radius value, we calculate the function $\nu_0(M_P)$ for various core masses between 0 $M_\oplus$ (solid red line) and 10 $M_\oplus$ (solid purple line). The figure includes an insert which zooms into the range $0.9 \leq M_P \leq 1.1\ M_J$. The gray area in the insert depicts the frequency range reached by ν_0 for the models with $R_P = 1.0\ R_J$ and $0 \leq M_{core} \leq 10\ M_\oplus$. The observed point for Jupiter has been added, both on the figure (black cross) and on the insert (with errorbars). The value of its characteristic frequency is taken from the measurements of Gaulme et al. (2011).

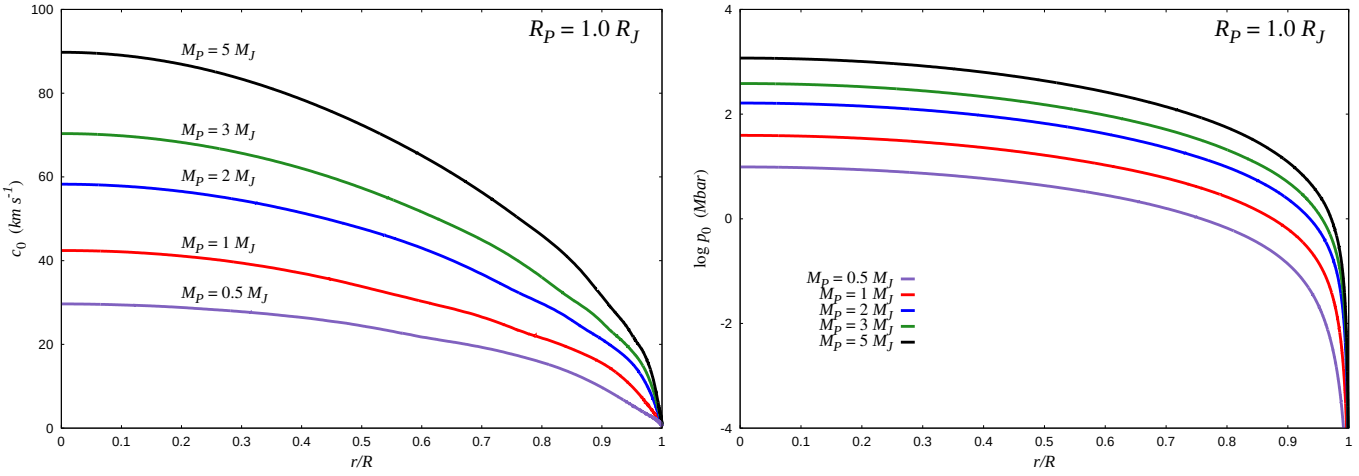

FIG. 7.— Left panel: distribution of sound speed c_0 $(km\ s^{-1})$ as a function of the relative radius r/R for coreless exoplanet models with various masses, with the radius fixed at $R_P = 1.0\ R_J$. Right panel: distribution of pressure p_0 $(Mbar)$ for the same models, with a logarithmic scale for the Y-axis. At every radius r, both the sound speed and the pressure are increasing functions of the planet mass, when the planet radius is fixed at $R_P = 1.0\ R_J$.

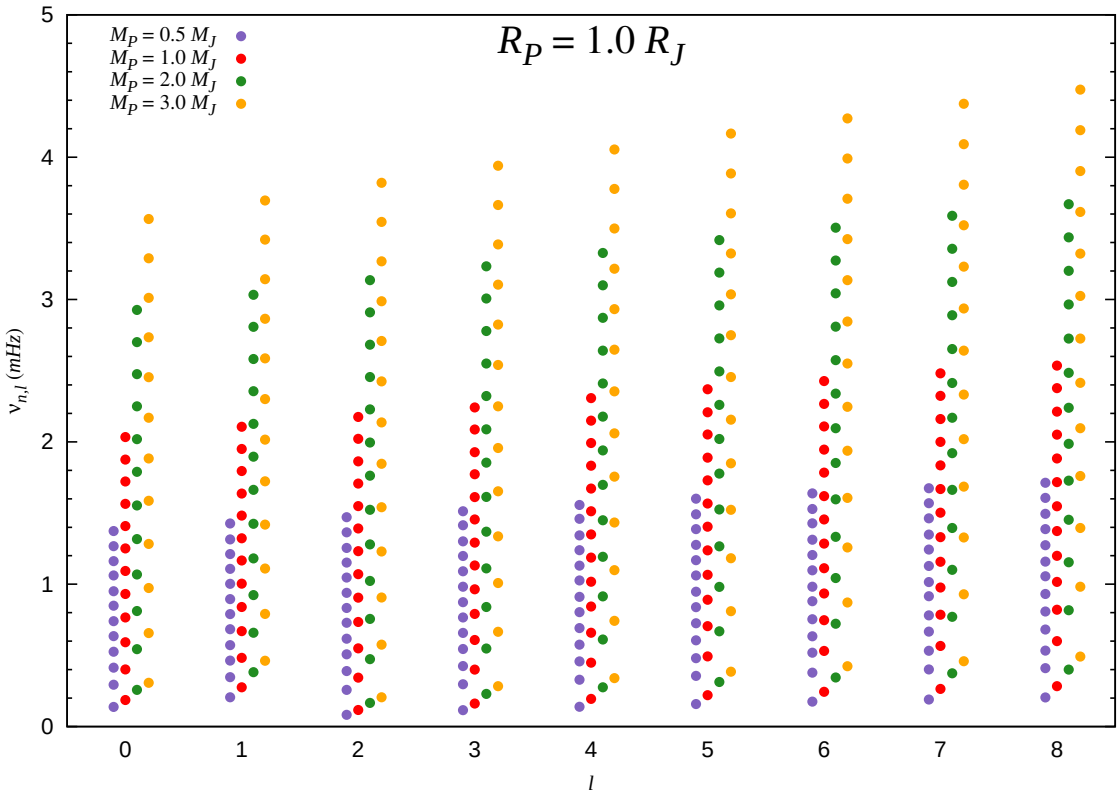

FIG. 8.— Low-order eigenfrequencies of oscillation modes (in mHz) as a function of the degree l for coreless exoplanet models with various masses, with the radius fixed at $R_P = 1.0\ R_J$. The helium mass fraction in the envelope is 0.25. For the sake of clarity, the eigenvalue dots of the different models has been seperated and drawn on both sides of each integer degree l.

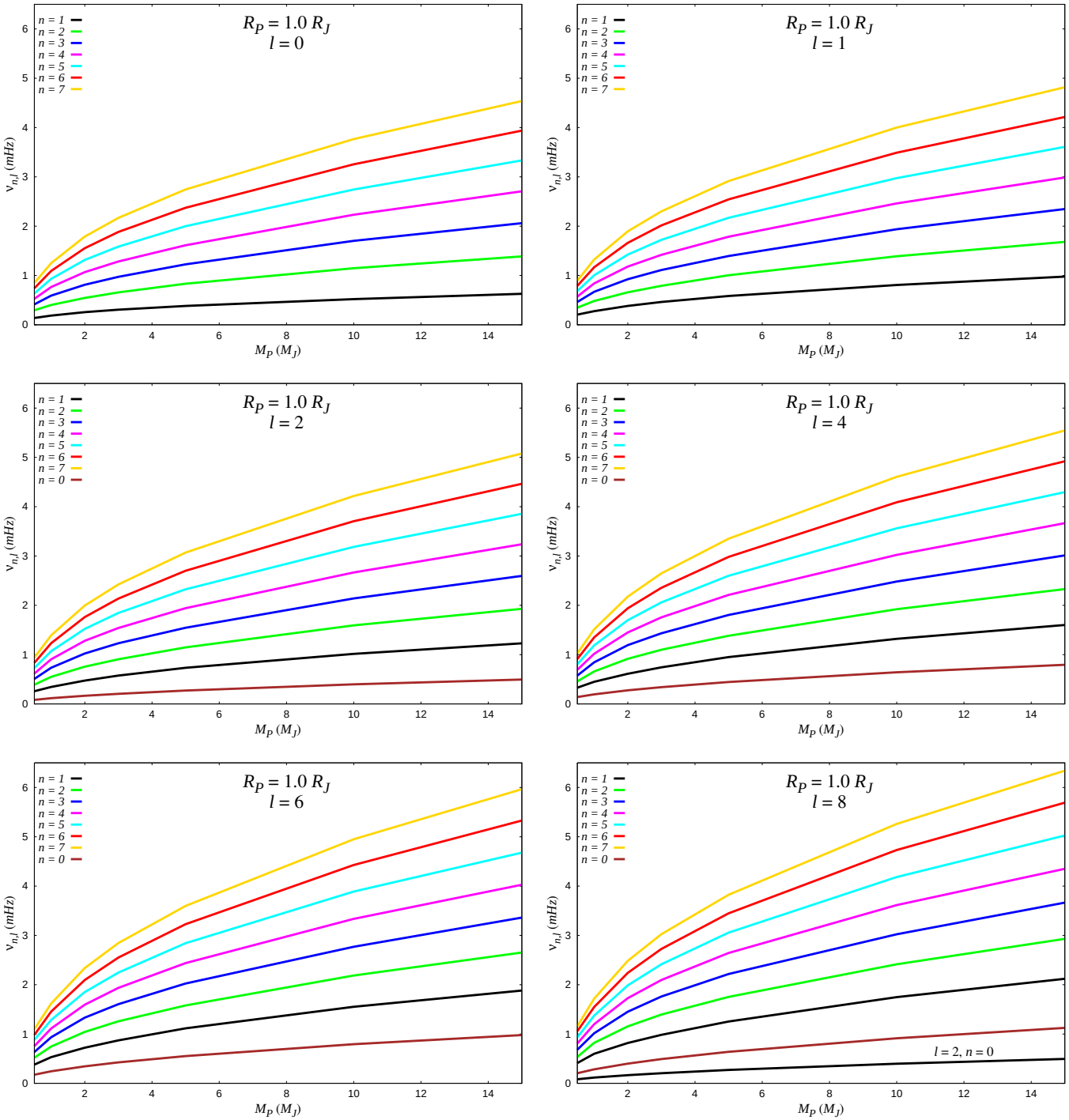

FIG. 9.— Eigenfrequencies of oscillation modes (in mHz) as a function of the planet mass for coreless exoplanet models with the radius fixed at $R_P = 1.0\ R_J$, and for various values of the degree l. For the represented modes, for each value of the planet mass M_P, the frequency minimum and maximum are obtained for $(n, l) = (0, 2)$ (middle left panel) and $(n, l) = (7, 8)$ (bottom right panel), respectively. On the bottom right panel ($l = 8$), the functions $\nu_{0,2}(M_P)$ has been added (black dashed line). Thus, the frequency range of the calculated modes is contained within the solid gold line, defined by $(n, l) = (7, 8)$,and the black dashed line, defined by $(n, l) = (0, 2)$.

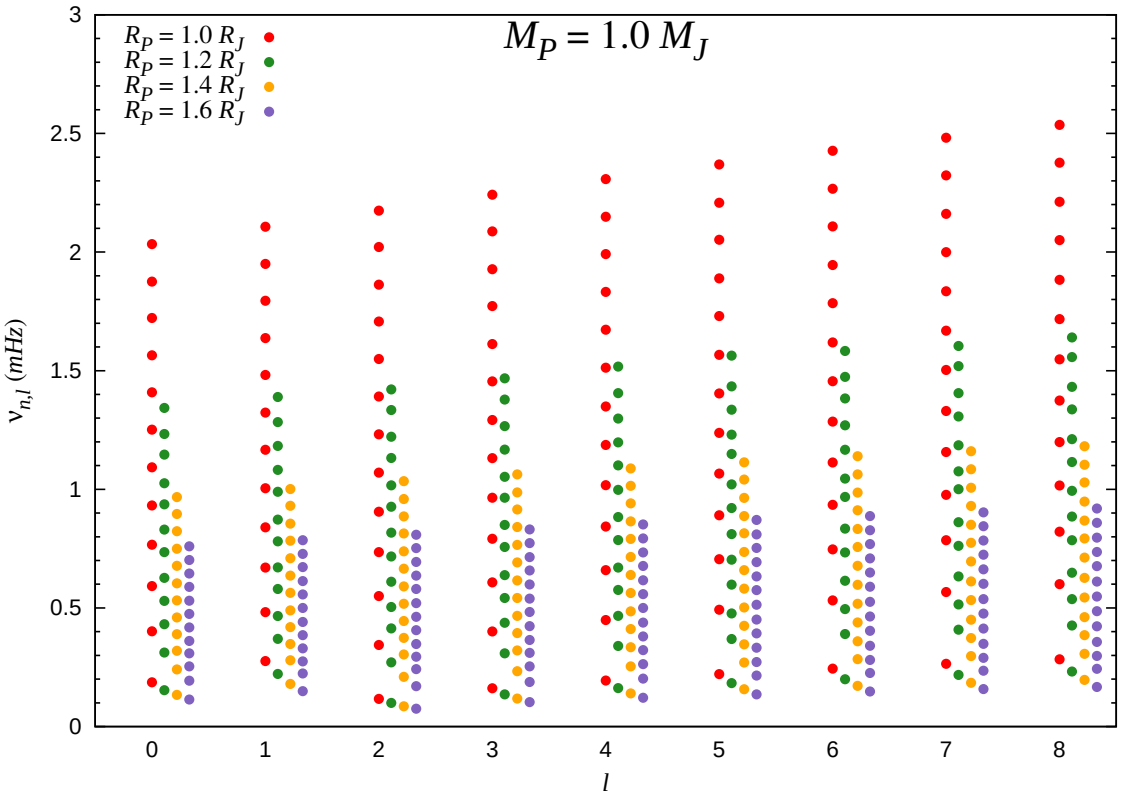

FIG. 10.— Eigenfrequencies of oscillation modes (in mHz) as a function of the degree l for exoplanet coreless models of various radii, with the mass fixed at $M_P = 1.0\ M_J$. The helium mass fraction in the envelope is 0.25. For the sake of clarity, the eigenvalue dots of the different models has been seperated and drawn in the vicinity of each integer degree l.

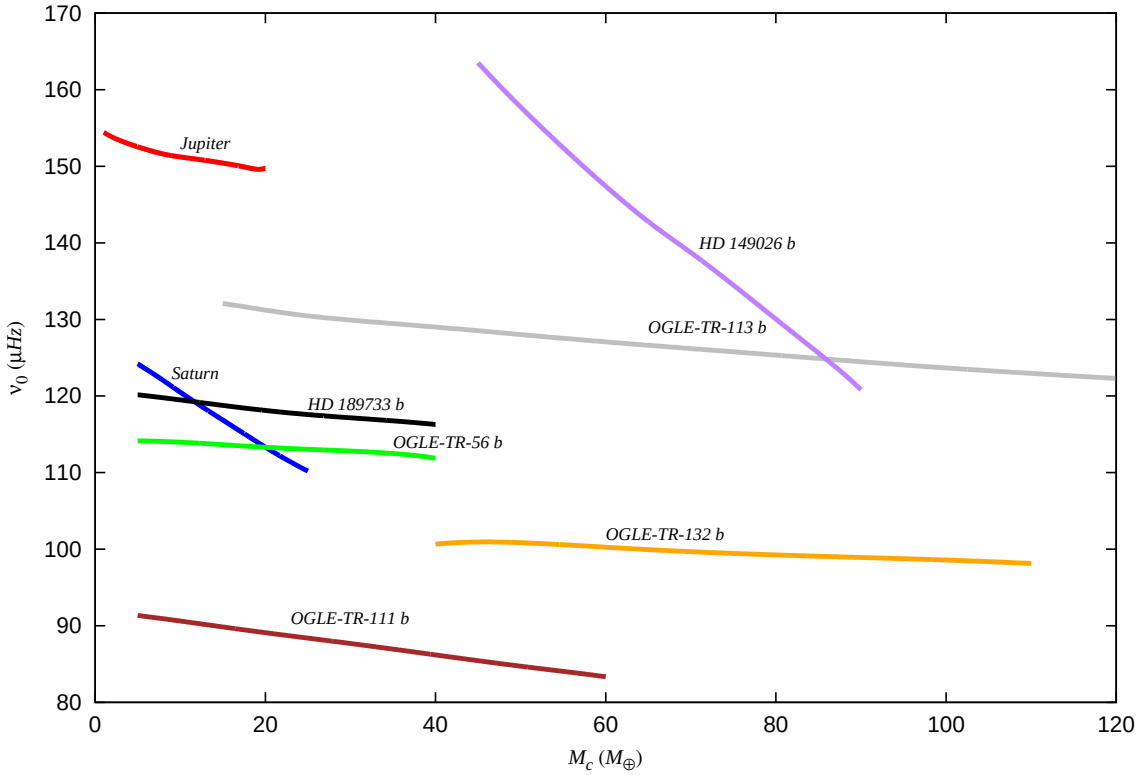

FIG. 11.— The charateristic frequency ν_0 as a function of the core mass, M_c, for various exoplanets. The helium mass fraction has been set equal to 0.25 in the envelope. The estimated range of core masses have been taken from various sources; Jupiter, Saturn: Saumon & Guillot (2004); HD149026b: Sato et al. (2005); for all the other planets: Burrows et al. (2007).

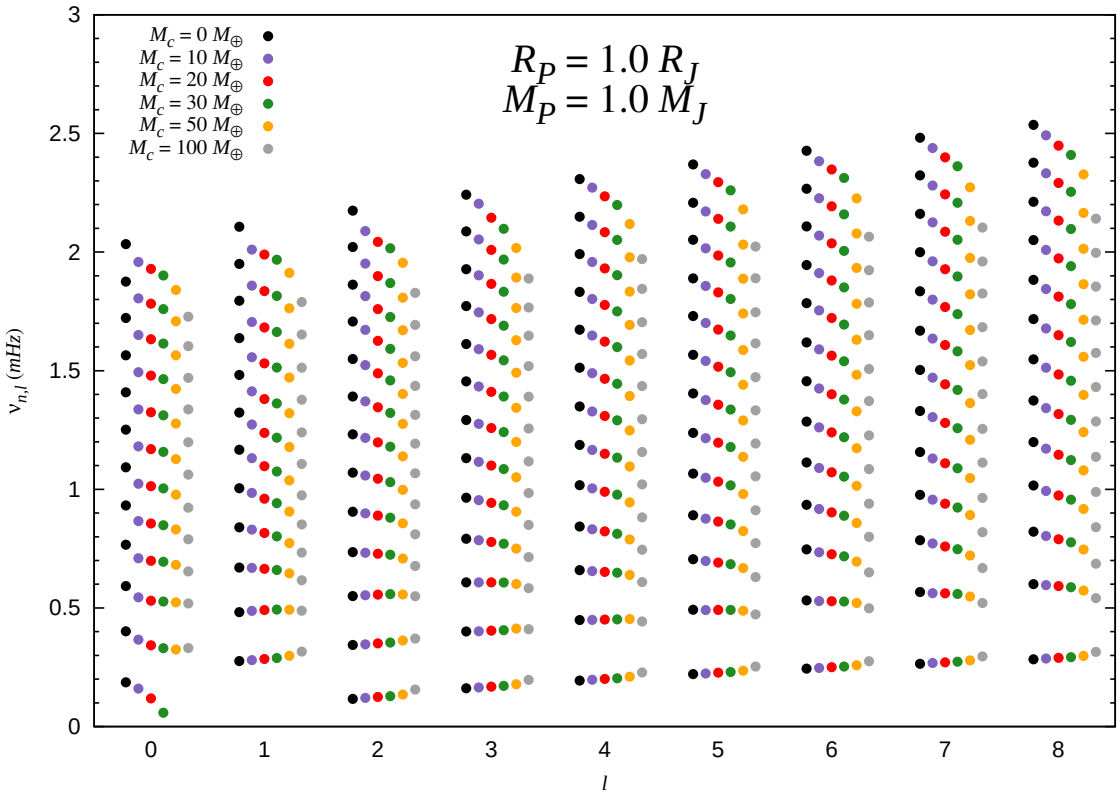

FIG. 12.— Low-order eigenfrequencies of oscillation modes (in mHz), as a function of the degree l, for exoplanet models with various core masses, with the radius fixed at $R_P = 1.0\ R_J$ and the mass fixed at $M_P = 1.0\ M_J$. The helium mass fraction in the envelope is 0.25. For the sake of clarity, the eigenvalue dots of the different models has been seperated and drawn on both sides of each integer degree l.

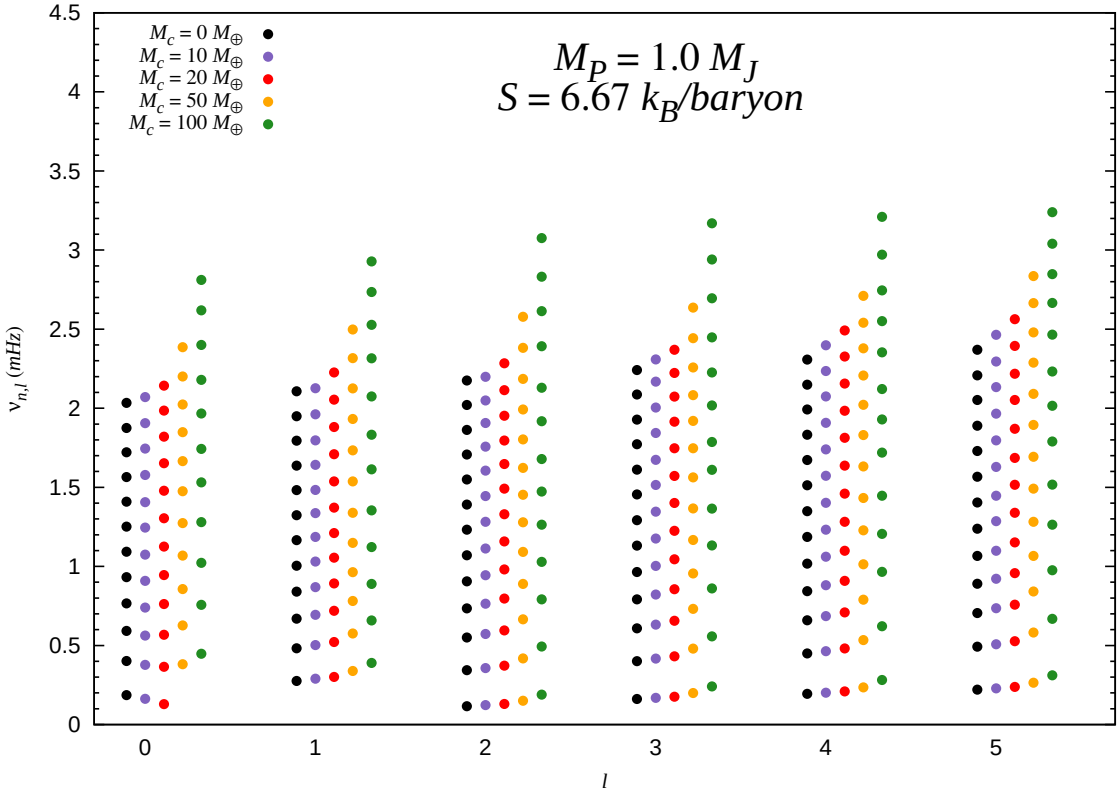

FIG. 13.— Low-order eigenfrequencies of oscillation modes (in mHz), as a function of the degree l, for exoplanet models with various core masses, with the radius fixed at $R_P = 1.0\ R_J$ and the specific entropy fixed at $S = 6.67 k_B/baryon$. The helium mass fraction in the envelope is 0.25. For the sake of clarity, the eigenvalue dots of the different models has been seperated and drawn on both sides of each integer degree l.

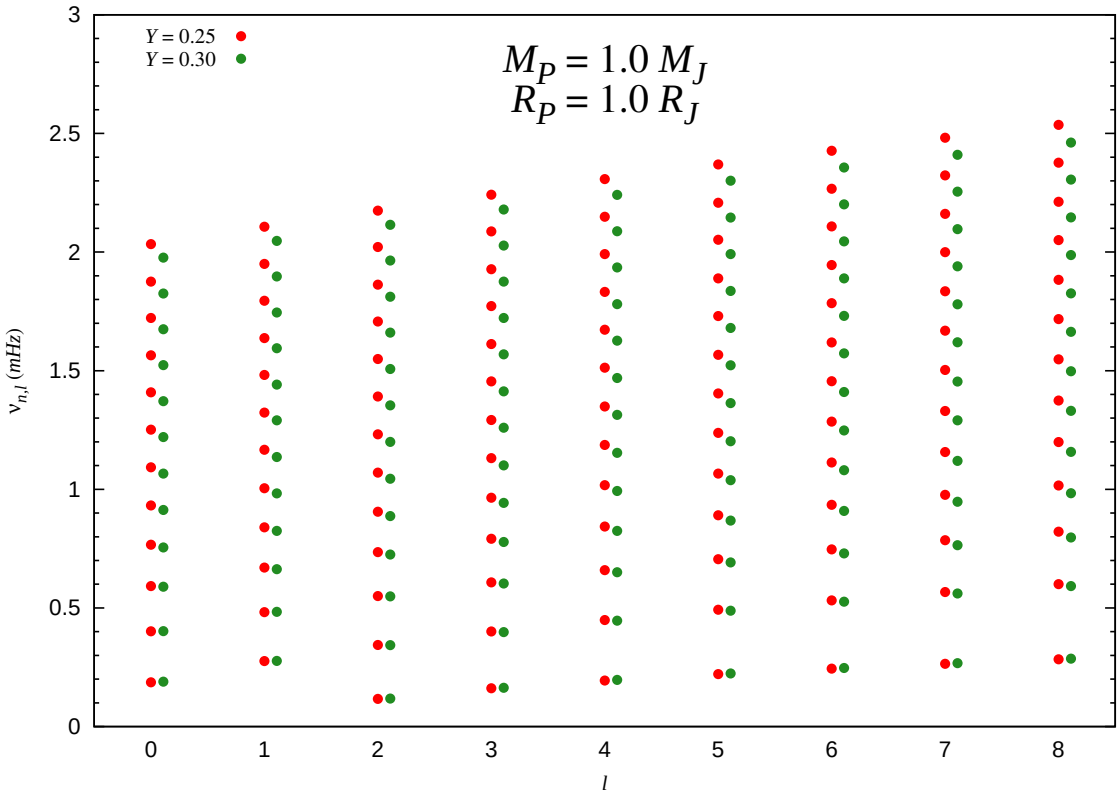

FIG. 14.— Low-order eigenfrequencies of oscillation modes (in mHz), as a function of the degree l, for exoplanet models with two different helium mass fractions Y in the envelope, with the radius fixed at $R_P = 1.0\ R_J$ and the mass fixed at $M_P = 1.0\ M_J$. For the sake of clarity, the eigenvalue dots of the different models has been seperated and drawn on both sides of each integer degree l.

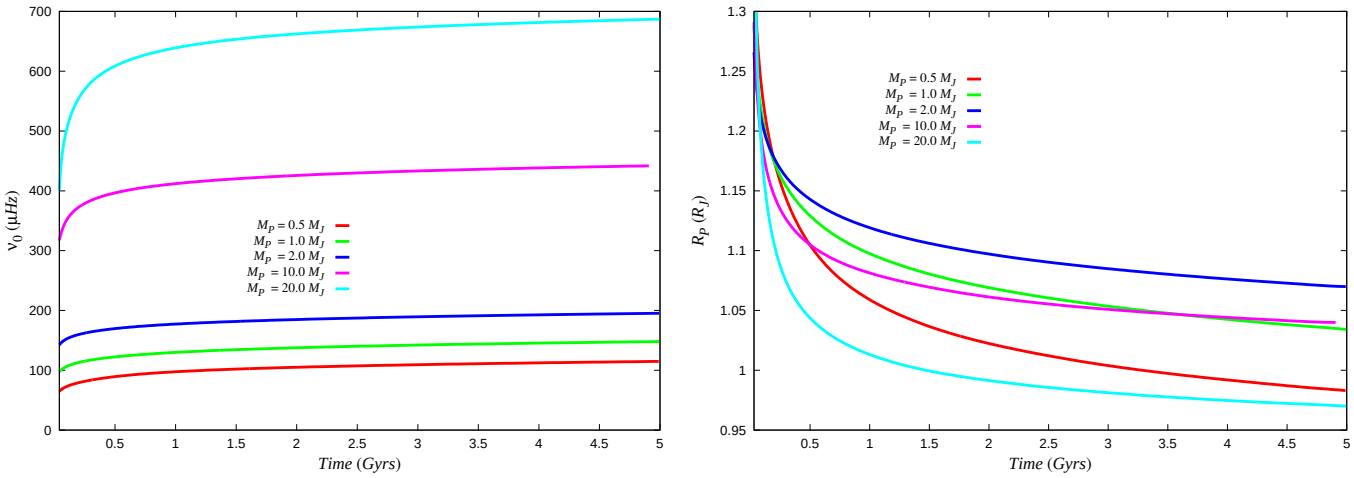

FIG. 15.— Left panel : the charateristic frequency ν_0 as a function of time for various coreless planetary models, characterized by their constant mass (M_P = 0.5, 1.0, 2.0, 10.0 and 20.0M_J). The helium mass fraction has been set to 0.25 in the envelope. The planets are considered in isolation during their evolution, which means that no irradiation is taken into account. Right panel: The corresponding evolution of the planet radius for the same coreless planetary models, in Jupiter units. The X-axis does not begin at the origin.